Applied and Computational Mechanics 20 (2026) XXX–YYY

Comparative probabilistic fragility assessment of a 10-storey fixed-base and friction-pendulum base-isolated RC frame under near- and far-field earthquake motions

D. Pateliya[a], A. Thoriya[a], H. Rangwala[a,*], T. Vora[a]

[a] *Department of Civil Engineering, Marwadi University, Rajkot, India*

Received 19 June 2025; accepted 19 June 2026

Abstract

This study conducts a comparative probabilistic fragility assessment of a representative 10-storey reinforced concrete (RC) frame considered in fixed-base and friction-pendulum base-isolated configurations under near- and far-field earthquake motions. A collection of 44 seismic records, grouped into far-field (FF), near-field with fling-step effect (NFFS), near-field with directivity effect (NFD) and elevated peak ground acceleration (PGA) to peak ground velocity (PGV) ratio (NFD-GT-150, >150 cm/s/g), and near-field with directivity effect and reduced PGV/PGA ratio (NFD-LT-150, <150 cm/s/g), was analysed. Using incremental dynamic analysis (IDA) and probabilistic seismic demand modelling (PSDM), vulnerability curves were constructed for five structural response metrics: maximum interstorey drift ratio (IDR_{max}), maximum roof drift ratio (RDR_{max}), maximum top floor acceleration (RA_{max}), maximum base shear force (BS_{max}), and maximum isolator displacement (ID_{max}), spanning four damage levels: slight, moderate, extensive, and collapse. Findings indicate that proximate seismic excitations (NFD-GT-150, NFFS) substantially elevate vulnerability across all damage levels, with NFD-GT-150 yielding the highest probabilities of exceedance (e.g., 99.38 % for fixed-base collapse at $0.8g$ PGA). Base isolation decreased IDR_{max} by up to 88.1 % at the collapse level under FF at $0.2g$ PGA, though its efficacy waned under NFD-GT-150 conditions. IDR_{max} and ID_{max} emerged as the most responsive metrics, consistently displaying elevated exceedance probabilities. The PGV/PGA ratio proved a vital predictor of seismic damage, with NFD-GT-150 raising collapse exceedance probability by 32.5 % over NFD-LT-150 at $0.4g$ PGA for base-isolated frames. These insights stress the importance of integrating PGV/PGA considerations and proximate seismic effects into design standards to bolster the durability of base-isolated structures in fault-proximate zones. Since the investigation is limited to one 10-storey regular RC frame, the results should be interpreted as a detailed case-study assessment rather than as generalized conclusions for all RC building heights and configurations.
© 2026 University of West Bohemia in Pilsen.

Keywords: base isolation, earthquake ground motion, fragility analysis, friction pendulum bearing, PGV/PGA ratio

1. Introduction

Seismic activities pose substantial risks to structural stability and economic resources, with significant impacts evident in seismically active areas like India, where the 2001 Bhuj earthquake underscored the demand for resilient construction approaches [29]. Conventional earthquake-resistant design aims to avoid complete structural failure but frequently allows damage to non-load-bearing components, resulting in excessive interstorey movements or accelerations that impair the post-event functionality of critical facilities such as hospitals [16]. Base isolation offers a strategy to decouple structures from ground shaking, diminishing energy transmission

*Corresponding author. Tel.: +91 972 690 49 99, e-mail: husain.rangwala@marwadieducation.edu.in.
https://doi.org/10.24132/acm.2026.1018

Article in Press

Nomenclature

BI	base-isolated	IM	intensity measure
BS	base shear	IM_m	median of IM
BS_{max}	maximum of BS	NFD	near-field with directivity effect
DS	damage state	NFFS	near-field with fling-step effect
EDP	engineering demand parameter	PGA	peak ground acceleration
FB	fixed-base	PGV	peak ground velocity
FF	far-field	POE	probability of exceedance
FPB	friction pendulum bearing	PSDM	probabilistic seismic demand modelling
GM	ground motion		
IDA	incremental dynamic analysis	RA	roof acceleration
ID	isolator displacement	RA_{max}	maximum of RA
ID_{max}	maximum of ID	RC	reinforced concrete
IDR	interstorey drift ratio	RDR	roof drift ratio
IDR_{max}	maximum of IDR	RDR_{max}	maximum of RDR

and prolonging the natural period of the system [31]. Among isolation technologies, friction pendulum bearings (FPBs) are valued for their enduring strength, stability and self-centering capability, achieved through a sloped sliding surface that regulates the isolation period via pendulum-like motion [37].

Research into base-isolated structures highlights their success in managing distant seismic events. In [4], Bhandari er al. showed that base isolation reduces damage risk in far-field contexts but encounters difficulties with near-fault shocks when the peak ground velocity (PGV) to peak ground acceleration (PGA) ratios surpass 150 cm/s/g. In [15], Jangid improved FPB designs for near-fault conditions, finding that elevated friction levels decrease isolator displacement while sustaining superstructure integrity, though near-fault pulses challenge isolation efficiency. Previous studies have also shown that FPBs can effectively limit interstorey drift under far-field motions, although their performance may be adversely affected by near-fault directivity pulses [15, 16]. Seismic events within 15 km of a fault generate rapid pulses and directivity or fling-step phenomena, pushing structures into nonlinear responses even at low PGA levels [16]. In [24], Petti et al. noted that vertical near-fault motions enhance base shear in FPB-supported buildings, requiring advanced design considerations.

Fragility analysis provides a probabilistic approach to estimate damage exceedance across seismic intensities [5]. Bakhshi and Mostafavi [2] constructed fragility profiles for base-isolated reinforced concrete (RC) structures, indicating lower vulnerability under far-field conditions but greater exposure to near-fault excitations. In [20], Mazza et al. studied the effect of the near fault ground motion on an irregular RC frame structure isolated by FPBs. Wang et al. [36] further showed that large-strain effects can significantly influence the seismic response of isolated buildings subjected to near-fault earthquakes. Nevertheless, vulnerability evaluations of FPB-equipped RC frames under near-fault conditions, especially concerning PGV/PGA ratios and detailed damage metrics, such as maximum interstorey drift ratio (IDR_{max}), maximum roof drift ratio (RDR_{max}), maximum isolator displacement (ID_{max}), maximum roof acceleration (RA_{max}), and maximum base shear (BS_{max}), remain insufficient [4], a critical gap given the unique challenges posed by impulsive forces in fault-proximate regions [16].

Recent studies have shown that the seismic performance of base-isolated structures can

Article in Press

be strongly affected by near-fault ground-motion characteristics, particularly velocity pulses, fling-step effects, and the relationship between PGA and PGV [6, 32]. In [18], Liu et al. performed seismic fragility analysis of a base-isolated structure subjected to near-fault earthquakes using nonlinear finite element modelling and incremental dynamic analysis (IDA). Their results showed that the interstorey drift of the superstructure and the horizontal displacement of the isolation bearing increased significantly with seismic intensity, confirming the importance of IDA-based fragility assessment for isolated buildings under near-fault motions. Similarly, Nazarnezhad and Naderpour [22] investigated base-isolated RC moment frames subjected to near-fault pulse-like bidirectional seismic excitations and reported that pulse-period characteristics can significantly influence isolator displacement demand and damage probability.

The role of frequency-content-related parameters has also received increasing attention. In [10], Habib et al. compared base-isolated irregular RC structures subjected to pulse-like earthquakes with low and high PGA/PGV ratios and observed that the isolator response is significantly influenced by the PGA/PGV ratio and structural irregularity. Majdi et al. [19] further examined the correlation between near-fault pulse-like ground-motion characteristics and building vulnerability and reported that PGA and PGV show positive correlation with seismic response, while reliance on a single pulse-type earthquake parameter may be unreliable when limited ground-motion records are used. These studies support the need to explicitly consider PGV/PGA-related classification when assessing the fragility of base-isolated buildings.

Recent work has also emphasized the need to evaluate base-isolated systems using multiple demand parameters rather than only one structural response quantity. In [11], He et al. proposed a seismic-resilience assessment method for structures equipped with friction pendulum isolation bearings using two-dimensional fragility, in which both superstructure and bearing-level performance indexes were considered. Their study highlighted that one-dimensional fragility may not fully capture the coupled damage behaviour of the superstructure and isolation layer. Ebrahimi et al. [7] also showed that base-isolated systems may require supplemental damping or additional design considerations under near-fault conditions because isolation alone may not be sufficient to control displacement and pounding-related vulnerability. More recently, Kang et al. [17] evaluated base-isolated structures with different heights under far-fault, near-fault non-pulse, and near-fault pulse-type ground motions and reported that vibration-control effectiveness depends on structural height and ground-motion type.

Despite these developments, a limited number of studies have compared fixed-base and friction-pendulum base-isolated RC frames under systematically classified far-field, near-field directivity, and near-field fling-step records while simultaneously considering multiple engineering demand parameters (EDPs), such as the interstorey drift, roof drift, roof acceleration, base shear, and isolator displacement. This research addresses these gaps by conducting a comparative probabilistic seismic vulnerability evaluation of 10-storey fixed-base (FB) and base-isolated (BI) RC frames with FPBs under far-field (FF), near-field with high PGV/PGA ratio ($>$150 cm/s/g, NFD-GT-150), near-field with low PGV/PGA ratio ($<$150 cm/s/g, NFD-LT-150), and near-field with fling-step effect (NFFS) ground motions. The detailed methodology is explained in Fig. 1. The study aims to: (1) compare the probabilistic seismic response of FB and BI buildings under the ground-motion types mentioned above, (2) explore how PGV/PGA ratios affect damage likelihood, and (3) identify the most sensitive damage measure. IDA is employed to derive fragility curves for multiple damage measures across four damage states (slight, moderate, extensive, and collapse) using real earthquake records. The findings aim to enhance seismic design practices for buildings in near-fault zones, contributing to performance-based seismic design, and compare their performance with those in far-field zones.

Article in Press

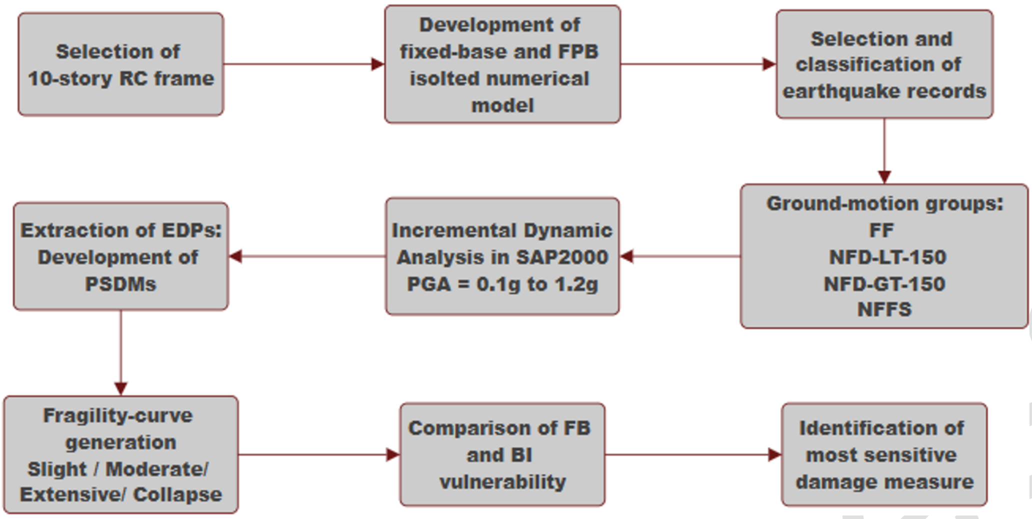

Fig. 1. Research methodology adopted for comparative fragility assessment of the fixed-base and friction-pendulum base-isolated 10-storey RC frame

The main innovation of this study lies in the integrated fragility-based comparison of a 10-storey RC frame in fixed-base and friction-pendulum base-isolated configurations under systematically classified far-field and near-field earthquake records. Unlike many previous studies that focus on either fixed-base or isolated structures, or consider only a limited number of response quantities, the present study evaluates both superstructure and isolation-system performance through five EDPs (IDR_{max}, RDR_{max}, RA_{max}, BS_{max}, and ID_{max}). Another important contribution is the explicit comparison of near-field directivity records with lower and higher PGV/PGA ratios, together with near-field fling-step records, within the same IDA-PSDM-based fragility framework. This allows the study to identify how velocity-pulse characteristics influence the vulnerability of fixed-base and FPB-isolated configurations and to determine the most sensitive damage measure for performance-based seismic assessment of the selected 10-storey RC frame.

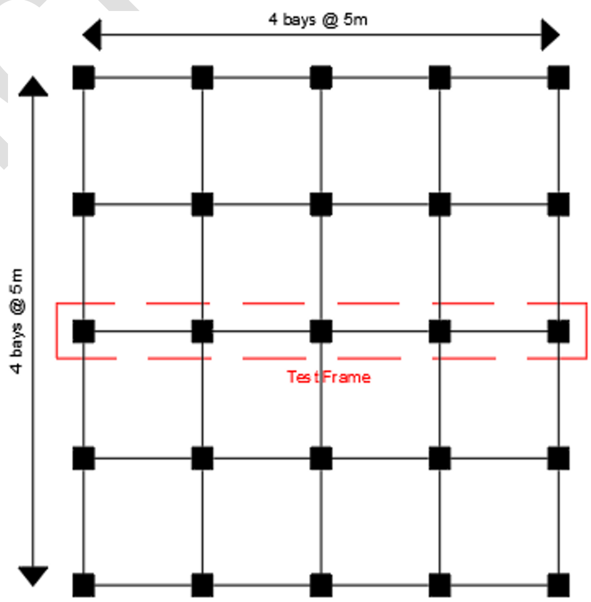

Fig. 2. Plan and elevation views of the 10-storey RC frame

2. Modelling and validation

This section outlines the modelling and design of FB and BI buildings, ground-motion selection, and model validation.

2.1. Modelling and design of the frames

A 10-storey FB building, a representative of typical office and residential buildings, was modelled as a two-dimensional (2D) internal frame, as shown in Fig. 2. The numerical modelling and nonlinear dynamic analyses of both the fixed-base and base-isolated configurations were carried out in SAP 2000. The building has a symmetric plan as shown in Fig. 2. Table 1 lists the loading and design properties of the FB building. To ensure a direct comparison between the FB and BI configurations, the superstructure member dimensions were kept unchanged in both models. The beam sections of 400 mm × 650 mm and column sections of 650 mm × 650 mm were used for both the fixed-base and FPB-isolated frames. Similarly, the material properties, loading, mass source, damping ratio, and nonlinear hinge definitions were kept identical. Therefore, the observed differences in the seismic response can be attributed mainly to the introduction of the friction pendulum bearing system rather than to changes in superstructure stiffness or strength. This modelling strategy is consistent with previous FPB frame studies, where the RC

Table 1. Modelling, design and loading parameters of the selected 10-storey RC frame

Material	Concrete	M30 grade	
	Steel	Fe 415 grade HYSD bars	
Frame modelling (designed as per IS 456 (2000) [12] and IS 1893 (2016) [13])	Beams	400 mm × 650 mm (for all storeys)	
	Columns	650 mm × 650 mm (for all storeys)	
	Column bases	Fixed	
	Frame infill	Bare frames (no infill considered)	
	Frame hinges	Beams	M3 (flexural hinges)
		Columns	P-M3 (uniaxial hinge)
		Auto-hinges as per ASCE table 41-13 at a relative distance from both ends	
Loading (considered as per IS 875)	Self-weight of members	25 kN/m^3 (considering weight per unit volume)	
	Dead load	1 kN/m^2 (on the floors)	
		1.5 kN/m^2 (on the top)	
	Live load	3 kN/m^2	
	Live load at the top floor	1.5 kN/m^2	
	Mass source	100% dead load and 25% live load	
	Seismic	Soil	Medium
		Zone	V
		Damping	5% structural damping
		Importance factor	1.5
	P-delta effect	Considered in the non-linear direct-integration time-history analyses	

Article in Press

frame is first designed as a fixed-base frame and then the isolated configuration is developed by introducing the friction pendulum isolation system without changing the superstructure member sections [3, 26, 35]. Material properties include a concrete compressive strength of 30 MPa, steel HYSD bars 415 MPa, as per the Indian Standard IS 456 (2000) [12]. The seismic design followed the Indian Standard IS 1893 (2016) provisions [13], while the other loading conditions are listed in Table 1. For the seismic analysis, 100% dead load (DL) and 25% live load (LL) were used. Plastic hinges were assigned at the beam and column ends at relative lengths of 0 and 1.0, following the guidelines in FEMA 356 [8]. Beams were assigned moment (M3) hinges to account for bending, while columns were assigned P-M3 hinges to capture axial force and moment interactions. Hinge properties were defined according to FEMA 356, enabling the simulation of nonlinear behaviour under seismic loading. The FB and BI frames were modelled to compare their seismic responses, with the FB model serving as a baseline.

2.2. Modelling and design of friction pendulum bearings (FPBs)

The base-isolated frame utilises FPBs to lengthen the structural period and absorb seismic energy via oscillatory dynamic behaviour [37]. Each FPB comprises a lower curved plate, an upper support, and a low-friction Teflon-coated sliding component to reduce resistance. The isolation period T depends on the sliding surface's radius of curvature R as

$$T = 2\pi\sqrt{\frac{R}{g}}, \tag{1}$$

where $g = 9.81\,\text{m/s}^2$ is the acceleration due to gravity. The horizontal force F on the bearing and the effective stiffness K_{eff} are given as

$$F = \frac{W}{R}u + \mu W, \qquad K_{\text{eff}} = \frac{W}{R} + \frac{\mu W}{u}, \tag{2}$$

where u is the horizontal displacement. In $(2)_1$, the first term represents the restoring force due to pendulum action, while the second term represents the frictional resistance. The FPB parameters were selected based on the target isolation period, tributary vertical load, typical sliding-interface properties and numerical stability requirements. The radius of curvature R was calculated from the target isolation period of 3 s using (1). The vertical load W on each bearing was obtained by dividing the total vertical load transferred to the isolation level by the number of isolators. The friction coefficient μ was selected as 0.05, which is commonly adopted for Teflon-steel sliding interfaces [15] and provides hysteretic energy dissipation through sliding friction. The initial stiffness $K_1 = W/R \approx 663\,\text{kN/m}$, post-yield stiffness $K_2 = W/R$, and yield displacement of 0.254 mm were defined based on experimental data for Teflon sliders [9, 21]. Vertical stiffness was set to 100 000 kN/m to reflect the slider's high rigidity. Damping was incorporated through the hysteretic loop, with the friction coefficient providing consistent energy dissipation across seismic intensities.

Model validation was performed by simulating the displacement response of a 5-storey base-isolated RC frame subjected to the 1940 El Centro earthquake and comparing it with the corresponding response reported by Jangid in [14]. The validation model was developed using the same basic structural properties reported in the reference study, including a floor mass of 50 000 kg and a structural period of 0.5 s. Fig. 3a presents the displacement-time response obtained from the current SAP2000 model, whereas Fig. 3b shows the corresponding response

Article in Press

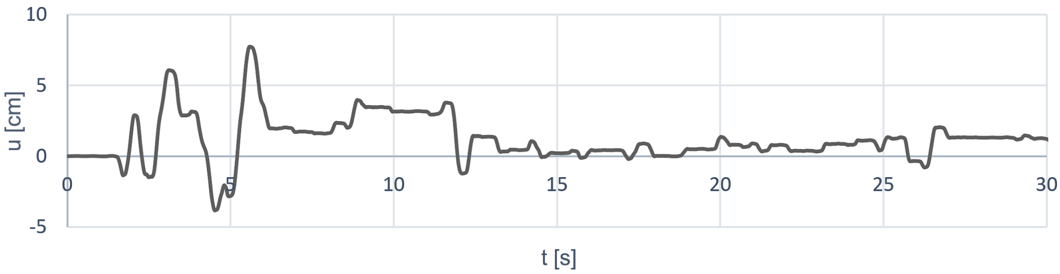

(a) current study using SAP 2000

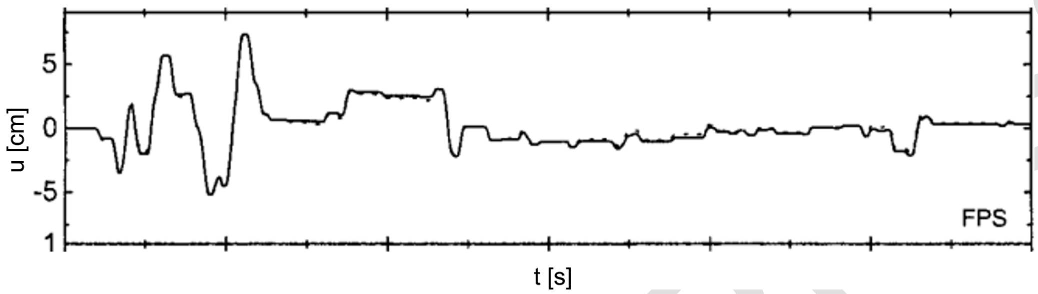

(b) reference data from [14]

Fig. 3. Displacement-time responses

adapted from [14]. The comparison indicates that the present model captures a similar displacement range and an overall time-history trend. Therefore, the validation supports the suitability of the adopted FPB modelling approach for the subsequent nonlinear dynamic analyses. It should be noted that the comparison is based on the reported graphical response from the reference study [14]; therefore, the validation is intended as a model-verification check rather than a complete experimental validation.

2.3. Earthquake records

Four sets of real earthquake records were selected to represent different ground-motion characteristics: far-field records, near-field directivity records with lower PGV/PGA ratio (NFD-LT-150), near-field directivity records with higher PGV/PGA ratio (NFD-GT-150), and near-field fling-step records. Eleven records were selected in each category to maintain an equal number of records for all ground-motion groups and to enable a balanced comparison of the resulting IDA curves and fragility functions. Thus, a total of 44 earthquake records were used in the study. FF records, sourced from events >15 km from the epicentre with magnitudes of 6.5–7.36, exhibit low acceleration and long periods [4]. NF records, from events <15 km with magnitudes of 6.0–7.6, capture high-frequency pulses and directivity or fling-step effects [16]. Tables 2 to 5 show the characteristics of the considered ground motions, sourced from the PEER Ground Motion Database [23].

3. Fragility analysis method

This section outlines the methodology for conducting fragility analysis to assess the seismic vulnerability of the FB and BI buildings under FF and NF earthquakes. The process involves IDA to generate seismic response data, development of PSDMs, and derivation of fragility curves for multiple damage measures across various damage states.

Article in Press

Table 2. Far-field ground motions

Earthquake name	Year	Station name	Mag.	PGA (g)	PGD (cm)	PGV (cm/s)
Northwest Calif-02	1941	Ferndale City Hall	6.6	0.0631	1.6325	3.7848
Borrego	1942	El Centro Array #9	6.5	0.0659	4.3559	6.2002
Kern County	1952	Santa Barbara Courthouse	7.36	0.0897	3.4258	11.4065
San Fernando	1971	Fairmont Dam	6.61	0.0748	2.7891	5.1663
Friuli_ Italy-01	1976	Barcis	6.5	0.0292	1.2574	2.3287
Tabas_ Iran	1978	Ferdows	7.35	0.0931	2.2721	5.4226
Imperial Valley-06	1979	Coachella Canal #4	6.53	0.116	2.5762	12.8318
Borah Peak_ ID-01	1983	TRA-670 ATR Reactor Bldg(Bsmt)	6.88	0.0218	0.3346	1.5549
Taiwan SMART1(45)	1986	SMART1 E02	7.3	0.1358	6.7238	14.4215
Superstition Hills-02	1987	Calipatria Fire Station	6.54	0.1896	4.0586	16.4234
Loma Prieta	1989	APEEL 3E Hayward CSUH	6.93	0.0787	4.6412	6.1353

Table 3. Near-field ground motions with lower PGV/PGA ratio (NF-LT-150)

Earthquake name	Year	Station name	Mag.	PGA (g)	PGD (cm)	PGV (cm/s)
San Fernando	1971	Pacoima Dam (upper left abut)	6.61	1.219	38.9955	114.4127
Imperial Valley-06	1979	El Centro Array #5	6.53	0.5287	48.8564	48.8859
Morgan Hill	1984	Gilroy Array #6	6.19	0.2923	5.9425	36.4742
Superstition Hills-02	1987	Parachute Test Site	6.54	0.3843	17.8052	53.0308
Loma Prieta	1989	Gilroy Array #2	6.93	0.3227	18.4464	40.3505
Loma Prieta	1989	Saratoga – Aloha Ave	6.93	0.3262	33.313	45.9494
Cape Mendocino	1992	Petrolia	7.01	0.6616	33.1974	88.4668
Northridge-01	1994	Sylmar – Converter Sta East	6.69	0.8527	34.0098	120.9118
Northridge-01	1994	Sylmar – Olive View Med FF	6.69	0.6049	15.9873	77.51
Kobe_ Japan	1995	KJMA	6.9	0.8342	21.0722	91.059
Parkfield-02_ CA	2004	Parkfield - Cholame 2WA	6	0.3728	6.7007	44.7802

IDA was employed to evaluate the nonlinear dynamic response of the RC frame under varying earthquake intensities [34]. It involves subjecting the structure to a suite of ground-motion records scaled incrementally to capture the full range of behaviour, from an elastic response to collapse [33]. IDA was performed using SAP 2000 through nonlinear direct-integration time-history analysis. The selected earthquake records were scaled based on PGA from $0.1g$ to $1.2g$ at fixed increments of $0.1g$. The lower PGA level of $0.1g$ was selected to represent low-intensity excitation, whereas the upper level of $1.2g$ was selected to capture severe nonlinear response and collapse-level demand. Since the fragility assessment considers slight, moderate, extensive, and collapse damage states, the selected PGA range was required to generate sufficient

Article in Press

Table 4. Near-field ground motions with higher PGV/PGA ratio (NF-GT-150)

Earthquake name	Year	Station name	Mag.	PGA (g)	PGD (cm)	PGV (cm/s)
Imperial Valley-06	1979	EC County Center FF	6.53	0.2354	47.9817	73.348
Imperial Valley-06	1979	El Centro Array #10	6.53	0.1731	35.3751	50.6645
Irpinia_ Italy-01	1980	Bagnoli Irpinio	6.9	0.1897	13.7394	34.6899
Irpinia_ Italy-01	1980	Sturno (STN)	6.9	0.3205	29.3104	71.9192
Superstition Hills-02	1987	Parachute Test Site	6.54	0.4318	46.1484	134.2202
Erzican_ Turkey	1992	Erzincan	6.69	0.3867	31.9757	107.0853
Landers	1992	Lucerne	7.28	0.7252	113.8669	133.3341
Northridge-01	1994	Jensen Filter Plant Administrative Building	6.69	0.4105	44.6137	111.414
Kobe_ Japan	1995	Port Island (0 m)	6.9	0.3479	39.2859	90.6254
Duzce_ Turkey	1999	Duzce	7.14	0.4043	49.6713	71.1177
Cape Mendocino	1992	Bunker Hill FAA	7.01	0.1774	38.9849	67.8562

Table 5. Near-field fling-step (NFFS) ground motions

Earthquake name	Year	Station name	Mag.	PGA (g)	PGD (cm)	PGV (cm/s)
Chi-Chi	1999	TCU052	7.6	0.35	178	493.52
Chi-Chi	1999	TCU052	7.6	0.44	216	709.09
Chi-Chi	1999	TCU068	7.6	0.50	277.56	715.82
Chi-Chi	1999	TCU068	7.6	0.36	294.14	895.72
Kocaeli	1999	Yarimca	7.4	0.23	88.83	184.84
Kocaeli	1999	Izmit	7.4	0.23	48.87	95.49
Kocaeli	1999	Sakarya	7.4	0.41	82.05	205.93
Chi-Chi	1999	TCU072	7.6	0.36	66.73	245.3
Chi-Chi	1999	TCU072	7.6	0.46	83.6	209.67
Chi-Chi	1999	TCU065	7.6	0.76	128.32	228.41
Chi-Chi	1999	TCU071	7.6	0.63	79.11	244.05

demand data across the full damage-state spectrum. The fixed $0.1g$ interval also provides a uniform intensity-measure grid for developing PSDMs and comparing fragility curves between the fixed-base and FPB-isolated configurations. Five EDPs were monitored: $\mathrm{IDR}_{\mathrm{max}}$, $\mathrm{RDR}_{\mathrm{max}}$, $\mathrm{ID}_{\mathrm{max}}$, $\mathrm{RA}_{\mathrm{max}}$, and $\mathrm{BS}_{\mathrm{max}}$. These EDPs reflect damage to the superstructure, isolation system and overall seismic performance [4].

PSDMs were developed to relate the EDPs to the intensity measure (IM), specifically PGA, due to its widespread use in seismic hazard assessment [5]. The response data from IDA were assumed to follow a log-normal distribution, a common assumption in seismic fragility analyses [25]. For each EDP, a regression analysis of logarithmic values was performed yielding a linear relationship

$$\ln(\mathrm{EDP}) = \ln a + b \ln(\mathrm{PGA}), \tag{3}$$

where a and b are regression coefficients.

Fragility curves express the conditional probability of exceeding a damage state (DS) given

Article in Press

Table 6. Defined thresholds for damage states based on structural performance indicators (W indicates the total seismic weight calculated as per IS 1893 (2016) provisions, and D_{max} is the design displacement of the isolator)

Performance indicator	Slight	Moderate	Extensive	Collapse
IDR_{max}	0.05 %	0.10 %	0.20 %	0.70 %
BS_{max}	5 % W	10 % W	15 % W	20 % W
RDR_{max}	0.10 %	0.50 %	1.00 %	2.00 %
ID_{max}	$0.2D_{\text{max}}$	$0.4D_{\text{max}}$	$0.8D_{\text{max}}$	$1.2D_{\text{max}}$
RA_{max}	$0.1g$	$0.2g$	$0.3g$	$0.4g$

an IM and defined as

$$P(\text{DS}|\text{IM}) = \frac{1}{\beta_D}\Phi\big(\ln(\text{IM}) - \ln(\text{IM}_m)\big), \tag{4}$$

where Φ is the standard normal cumulative distribution function, IM_{m} is the median IM at which the EDP reaches the damage state threshold and β_{D} is the logarithmic standard deviation from the PSDM [25], which quantifies the dispersion in the demand, accounting for structural and seismic variability [33]. Fragility curves were generated using (4) for four damage states (slight, moderate, extensive, and collapse) based on engineering judgement and literature [8]. Threshold values for each EDP were defined as follows [4]: for IDR_{max}, thresholds ranged from 0.05 % (slight) to 0.7 % (collapse); for ID_{max}, thresholds were set relative to the design displacement (e.g., $1.2D_{\text{max}}$ for extensive). Table 6 shows the threshold values for all EDPs and DSs.

Fragility curves were generated for both the FI and BI frames, enabling a comparative assessment of their seismic vulnerability across the four earthquake sets, mentioned in Section 2.3. This approach quantifies the influence of NF ground motion effects (e.g., high PGV/PGA ratios, fling-step) on the probability of exceedance (POE) for each damage measure.

4. Comparative fragility assessment of BI and FB buildings under varying ground-motion types

This section presents a detailed evaluation of seismic performance for 10-storey BI and FB buildings under FF, NFD-LT-150, NFD-GT-150, and NFFS ground motions (GMs). The assessment integrates IDA results with fragility curves, developed for five EDPs (IDR_{max}, RDR_{max}, RA_{max}, BS_{max}, and ID_{max}). These curves represent the conditional POE across four damage states (slight, moderate, extensive, and collapse) at PGA levels ranging from $0.1g$ to $1.2g$, averaged across each GM set. In the present study, IDA curves are used to evaluate the variation of selected EDPs with increasing PGA levels and to provide the demand data required for PSDM-based fragility-curve development.

4.1. Incremental dynamic analysis (IDA)

The IDA results for IDR_{max}, derived from nonlinear time-history analyses in SAP 2000, reveal distinct response patterns for FB and BI building across all GM types. For FB under FF, IDR_{max} increases gradually from 0 % at $0.0g$ PGA to approximately 5 % at $1.2g$ PGA, with a steep rise beyond $0.6g$ PGA, indicating progressive structural deformation as shown in Figs. 4 and 5. Previous studies have also demonstrated the effectiveness of IDA in analysing the performance

Article in Press

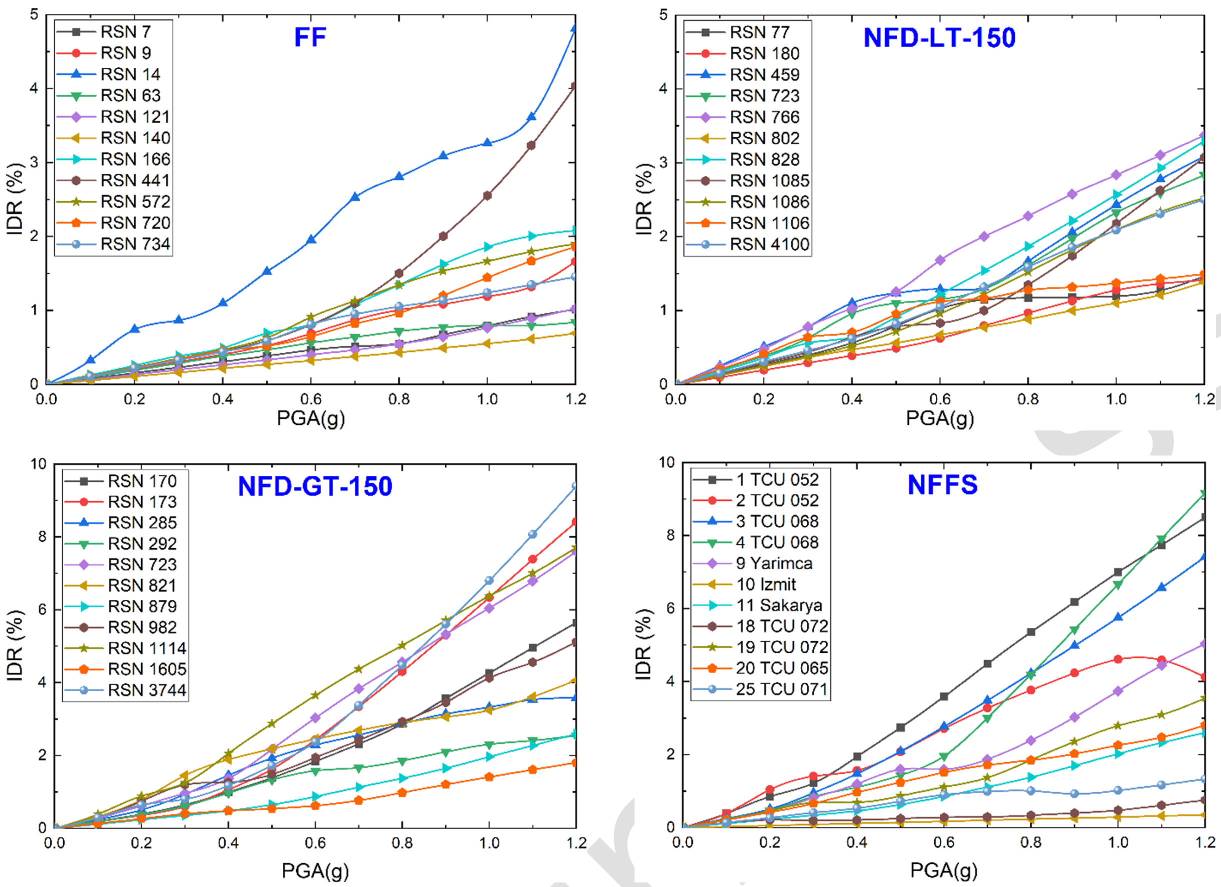

Fig. 4. IDA curves of interstorey drift ratio (IDR) for the FB building

of irregular buildings using nonlinear dynamic analysis [27,28]. Under NFD-LT-150, the curve shows a similar trend but with a slightly lower slope, peaking at around 4 % IDR_{max}, suggesting reduced intensity of deformation compared to FF. In contrast, NFD-GT-150 exhibits a sharper increase, reaching 10 % IDR_{max} at $1.2g$ PGA, reflecting heightened vulnerability due to velocity pulses. NFFS curves show the most rapid escalation, exceeding 8 % IDR_{max}, highlighting the impact of fling-step effects. For BI, IDR_{max} remains significantly lower, with FF curves peaking at 1.2 % and NFD-GT-150 reaching 1.1 % at $1.2g$ PGA, demonstrating the effectiveness of base isolation in limiting interstorey drift.

The BI building under NFD-LT-150 and NFFS shows IDR_{max} values of 1.0 % and 1.2 % at $1.2g$ PGA, respectively, indicating that while isolation mitigates drift, near-field effects still challenge performance. These IDA trends underscore the nonlinear behaviour of FB, where higher PGA levels trigger significant yielding, whereas BI maintains controlled deformation due to FPB damping. The observed differences correlate with fragility curves, where FB exhibits higher POE values (e.g., 99.99 % under NFD-GT-150 at $0.8g$ PGA) compared to BI (99.81 %), validating the IDA-derived reduction in structural demand.

The IDA analysis for maximum roof drift ratio (RDR_{max}) provides insight into the dynamic response at the roof level for FB and BI as shown in Figs. 6 and 7, respectively. For FB under FF, RDR_{max} increases from 0 % at $0.0g$ PGA to 3.5 % at $1.2g$ PGA, with a marked acceleration in the curve beyond $0.8g$ PGA, signaling the onset of significant roof displacement (see Fig. 8). Under NFD-LT-150, RDR_{max} reaches approximately 2.5 % at $1.2g$ PGA, showing a moderated increase compared to FF due to lower pulse intensity. NFD-GT-150 and NFFS, however, drive RDR_{max}

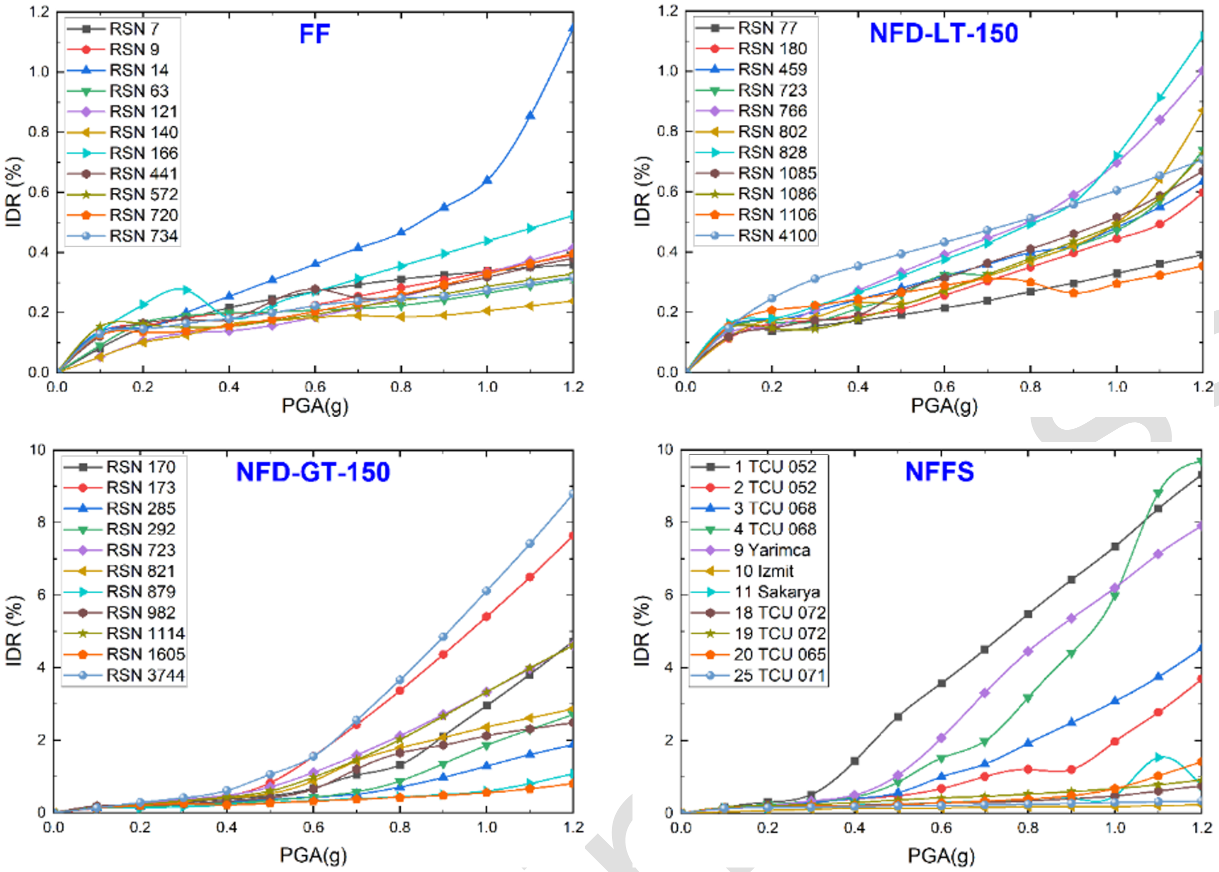

Fig. 5. IDA curves of interstorey drift ratio (IDR) for the BI building

to 6 % and 8 %, respectively at 1.2g PGA, with NFFS exhibiting a steeper slope from 0.4g PGA onward, indicative of fling-step-induced roof motion. For BI, RDR_{max} remains constrained, peaking at 0.4 % under FF, 0.5 % under NFD-LT-150, 0.6 % under NFD-GT-150, and 0.6 % under NFFS at 1.2g PGA, demonstrating the effectiveness of the isolation system in stabilising roof dynamics across all GM types.

The RDR_{max} of the BI building under NFFS (0.6 % at 1.2g PGA) compared to FB (8 %) highlights a substantial reduction, although the slight rise under NFD-GT-150 (0.6 %) suggests sensitivity to high-velocity pulses. This differential response is attributed to the FPBs' energy dissipation, which limits roof displacement even under intense GM. The IDA results align with fragility outcomes, where POE for FB and RDR_{max} reaches 63.9 % under NFD-GT-150 at 0.8g PGA, while POE for BI drops to 0.01 %, reflecting the success of the isolation system in mitigating roof drift vulnerability. The gradual increase in RDR_{max} for BI under NFD-GT-150 and NFFS also indicates a threshold beyond which isolation benefits diminish, a trend mirrored in the fragility curves' higher POE at extreme PGA levels.

The IDA curves for maximum top floor acceleration (RA_{max}) uncover the acceleration dynamics for FB and BI buildings across all GM types, as show in Figs. 8 and 9. For FB under FF, RA_{max} rises from 0g at 0.0g PGA to 1.4g at 1.2g PGA, with a pronounced upturn after 0.6g PGA, reflecting intensified floor acceleration (see Fig. 13 (left)). NFD-LT-150 peaks at 1.2g, showing a steady increase, while NFD-GT-150 and NFFS reach 1.4g and 1.2g, respectively, with NFD-GT-150 exhibiting a steeper gradient from 0.4g PGA due to directivity pulses. For BI, RA_{max} is significantly reduced, ranging from 0.8g under FF to 0.9g under NFD-GT-150 at

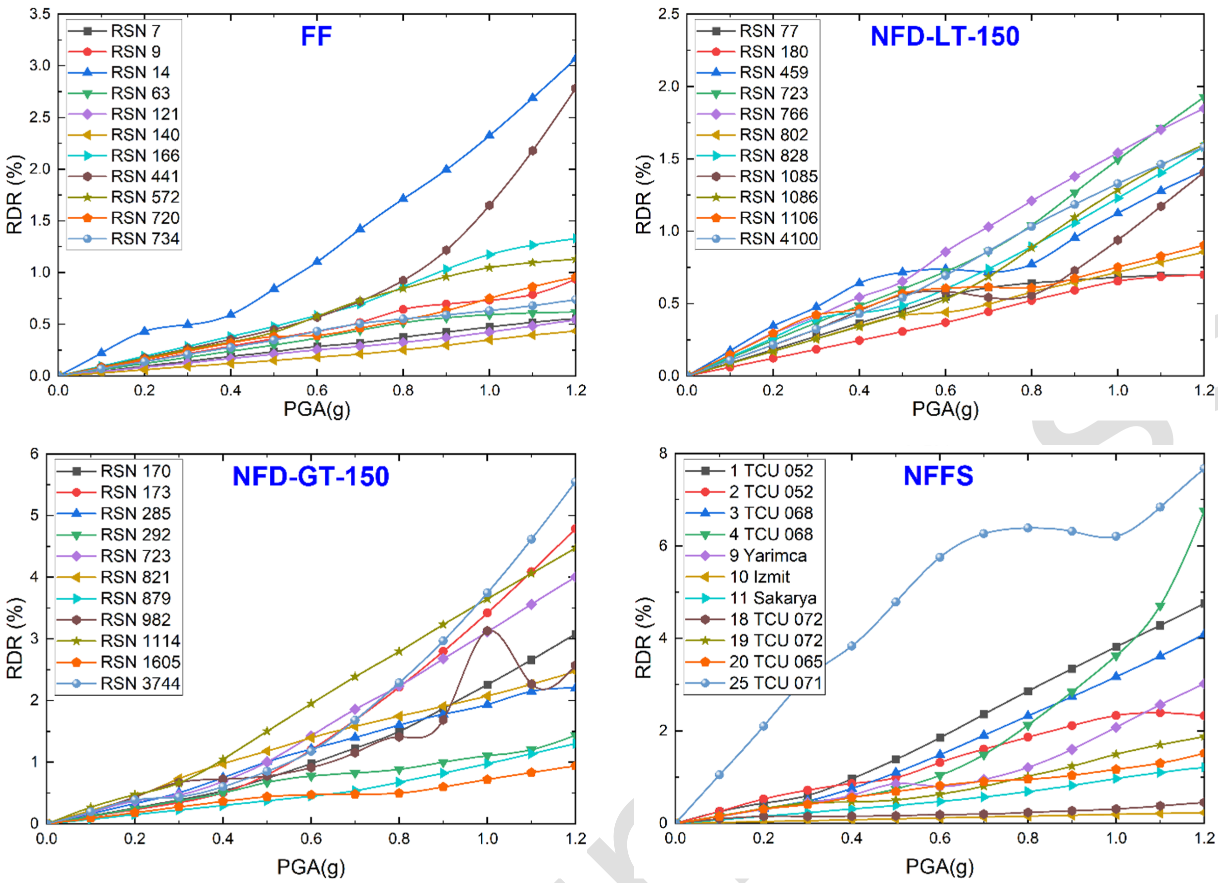

Fig. 6. IDA curves of roof drift ratio (RDR) for the FB building

1.2g PGA, with a gradual rise starting at 0.6g PGA, indicating effective damping by the isolation system. Under NFFS, RA_{max} for BI reaches 0.9g, suggesting a slight amplification due to fling-step effects.

The RA_{max} for BI under NFD-GT-150 (0.9g at 1.2g PGA) compared to the FB case (1.4g) underscores the ability of the isolation system to dampen acceleration, although the proximity for FB to 1.2g under NFFS indicates a limit to this benefit under extreme pulses. This behaviour is consistent with the fragility analysis, where POE for FB and RA_{max} is 99.91 % under NFD-GT-150 at 0.8g PGA, while in the BI case it is 69.17 %, reflecting IDA's evidence of reduced acceleration demand. The slight increase in the BI case under NFD-GT-150 and NFFS suggests that high-velocity GMs challenge the capacity of the isolation system, a nuance captured in the fragility curves' elevated POE at higher PGA levels, necessitating further design optimisation.

The IDA assessment for maximum base shear (BS_{max}) highlights shear force variations for FB and BI, as shown in Figs. 10 and 11. For FB under FF, BS_{max} increases from 0 % to 50 % of seismic weight at 1.2g PGA, with a sharp rise after 0.6g PGA, indicating significant base shear mobilisation (see Fig. 14 (left)). NFD-LT-150 peaks at 40 % BS_{max}, showing a moderated response, while NFD-GT-150 and NFFS reach 60 % and 80 %, respectively, with NFFS showing a rapid increase from 0.4g PGA due to fling-step effects. For BI, BS_{max} is lower, ranging from 20 % under FF to 50 % under NFD-GT-150 at 1.2g PGA, with a steady rise beginning at 0.6g PGA, reflecting the FPBs' shear reduction capacity. Under NFFS, BS_{max} for BI reaches 50 %, indicating a convergence with NFD-GT-150 due to intense GM loading.

The BS_{max} for BI under NFFS (50 % at 1.2g PGA) compared to FB (80 %) demonstrates

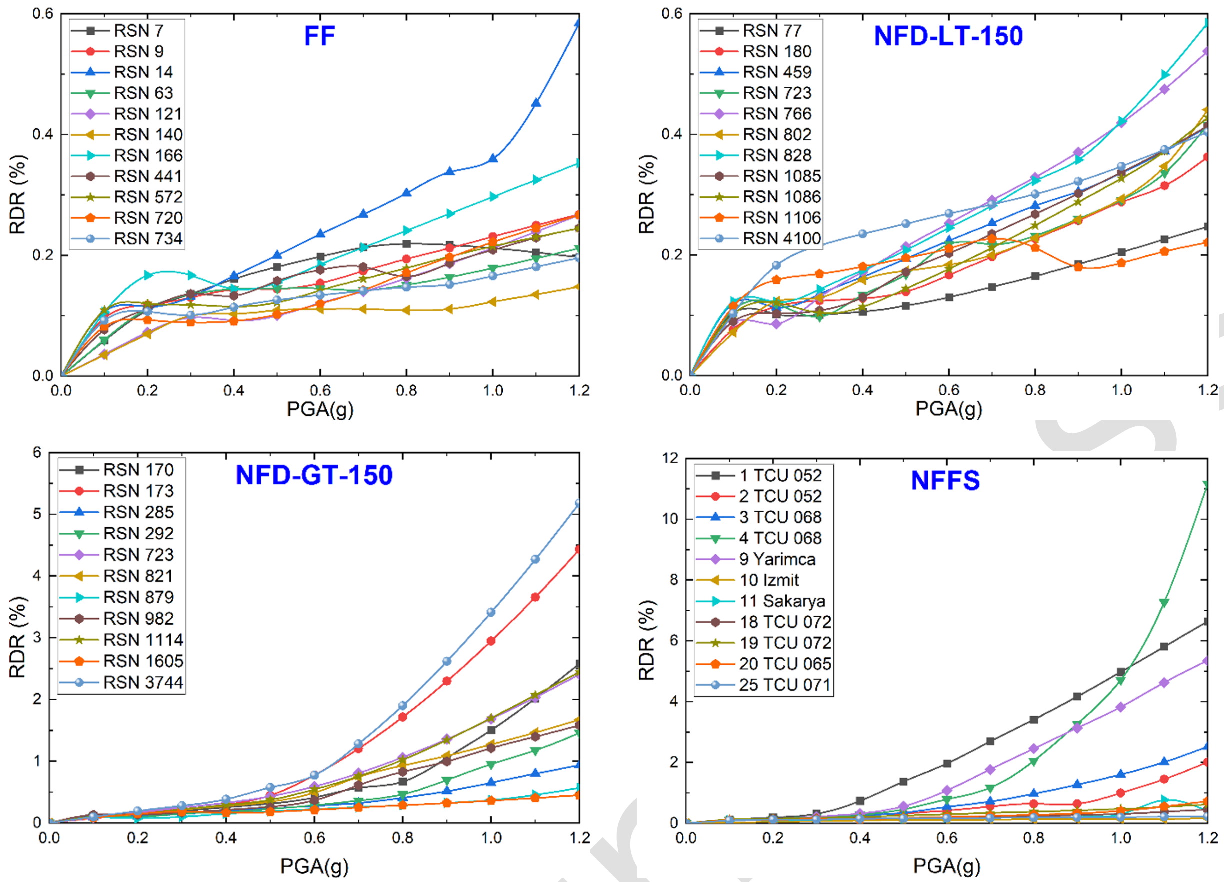

Fig. 7. IDA curves of roof drift ratio (RDR) for the BI building

a notable reduction, though the alignment with NFD-GT-150 (50 %) suggests pulse sensitivity. This is attributed to the FPBs' hysteretic damping, which limits shear force escalation under most conditions. The IDA results correlate with fragility data, where POE for FB and BS_{max} is 68.9 % under NFD-GT-150 at 0.8g PGA, while in the BI case it is is 18.97 %, validating the shear mitigation of the isolation system. The increased BS_{max} for BI under NFD-GT-150 and NFFS indicates a performance limit, consistent with fragility curves showing higher POE at extreme PGA levels, suggesting a need for enhanced isolation design.

4.2. Fragility analysis

The fragility curves, constructed from IDA data, provide a probabilistic measure of POE for FB and BI across the damage states, offering insights into structural vulnerability.

4.2.1. Maximum interstorey drift ratio (IDR_{max})

The fragility curves for IDR_{max}, as depicted in Fig. 12, reveal distinct vulnerability patterns across all GM types for FB and BI. Under FF, FB exhibits a POE of 98.00 % for slight damage at 0.2g PGA, increasing to 91.96 % for moderate, 94.49 % for extensive, and 23.40 % for collapse, indicating a gradual damage accumulation. BI reduces these values to 91.00 %, 74.11 %, 23.35 %, and 2.79 %, respectively, showcasing an 88.08 % reduction in collapse POE. Under NFD-LT-150, POE for FB reaches 99.99 % at 0.8g PGA for slight damage, with moderate at 99.99 %, extensive at 94.49 %, and collapse at 0.58 %, while BI shows 99.54 %, 97.31 %, 23.35 %, and 0.01 %, reflecting consistent isolation benefits. For NFD-GT-150, POE for FB

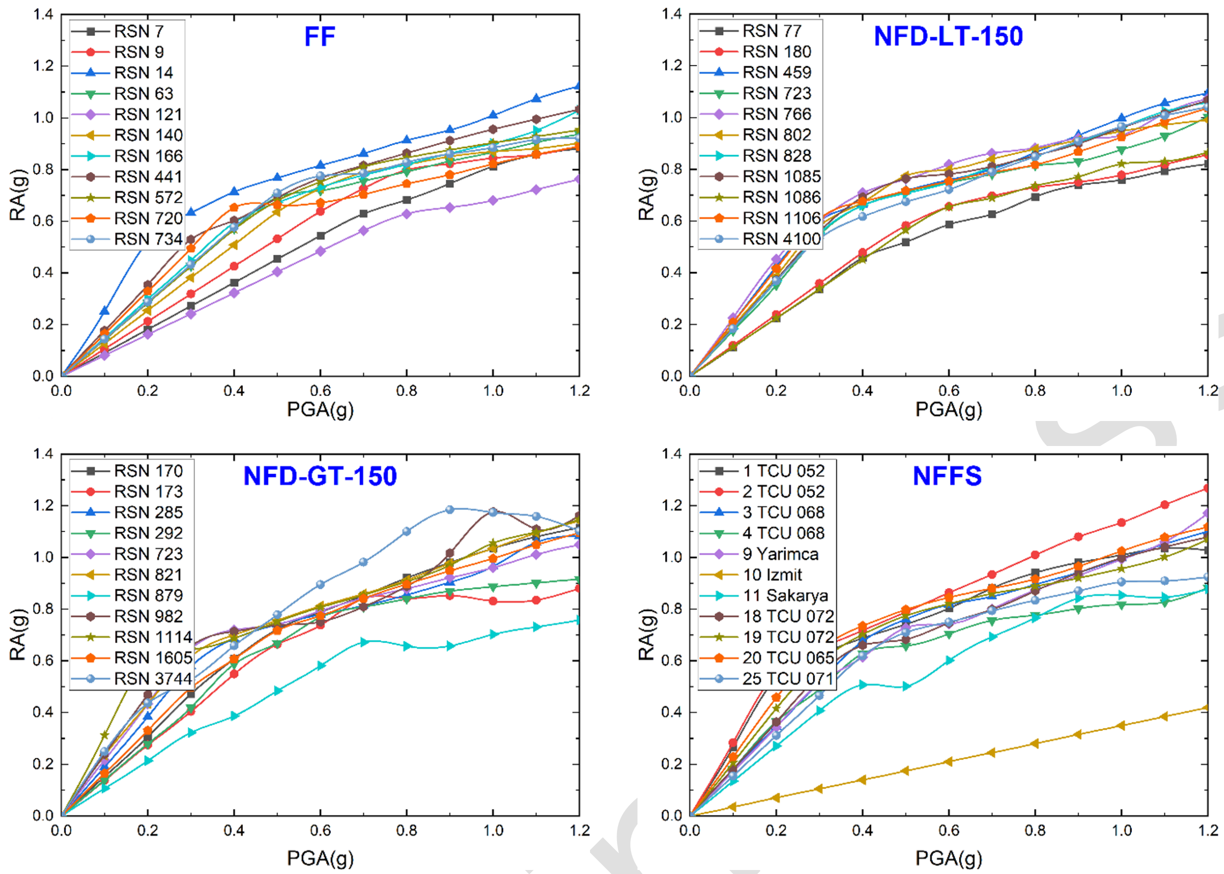

Fig. 8. IDA curves of roof accelerations (RA) for the FB building

peaks at 99.99 % for slight, 99.99 % for moderate, 97.17 % for extensive, and 99.05 % for collapse at $0.8g$ PGA, whereas values in the case of BI are 99.81 %, 98.63 %, 86.50 %, and 1.41 %, indicating a significant but diminishing reduction under high-velocity pulses. Under NFFS, POE for FB is 91.96 % for moderate, 57.75 % for extensive, and 23.09 % for collapse, while BI's are 74.11 %, 32.43 %, and 9.57 %, suggesting fling-step effects challenge isolation efficacy.

The accentuated POE gradients for the FB under NFD-GT-150 and NFFS, where collapse POE exceeds 99 % at $0.8g$ PGA, correspond with the IDA-observed IDR_{max} peaks of 10 % and 8 %, respectively, indicating an accelerated structural degradation under elevated seismic intensities. Conversely, the BI demonstrates more gradual POE trends, maintaining collapse POE below 10 % at $0.8g$ PGA, which aligns with IDA-recorded IDR_{max} values of 1.1 % to 1.2 %, underscoring the damping efficacy of FPBs. The transition from moderate to collapse damage states exhibits a steeper trajectory in FB under near-field GM, suggesting that seismic design standards should emphasise IDR_{max} threshold optimisation to enhance BI resilience in pulse-dominated regions, where isolation benefits are attenuated beyond a PGA threshold of $0.6g$.

4.2.2. *Maximum roof drift ratio (RDR_{max})*

Fig. 13 illustrates the RDR_{max} fragility curves, showing varied vulnerability across all GM types. Under FF, POE for FB and slight damage is 99.60 % at $0.2g$ PGA, rising to 72.29 % for moderate, 10.16 % for extensive, and 2.18 % for collapse, reflecting significant roof displacement. BI reduces these to 71.25 %, 22.62 %, 1.65 %, and 0.23 %, demonstrating effective isolation. For

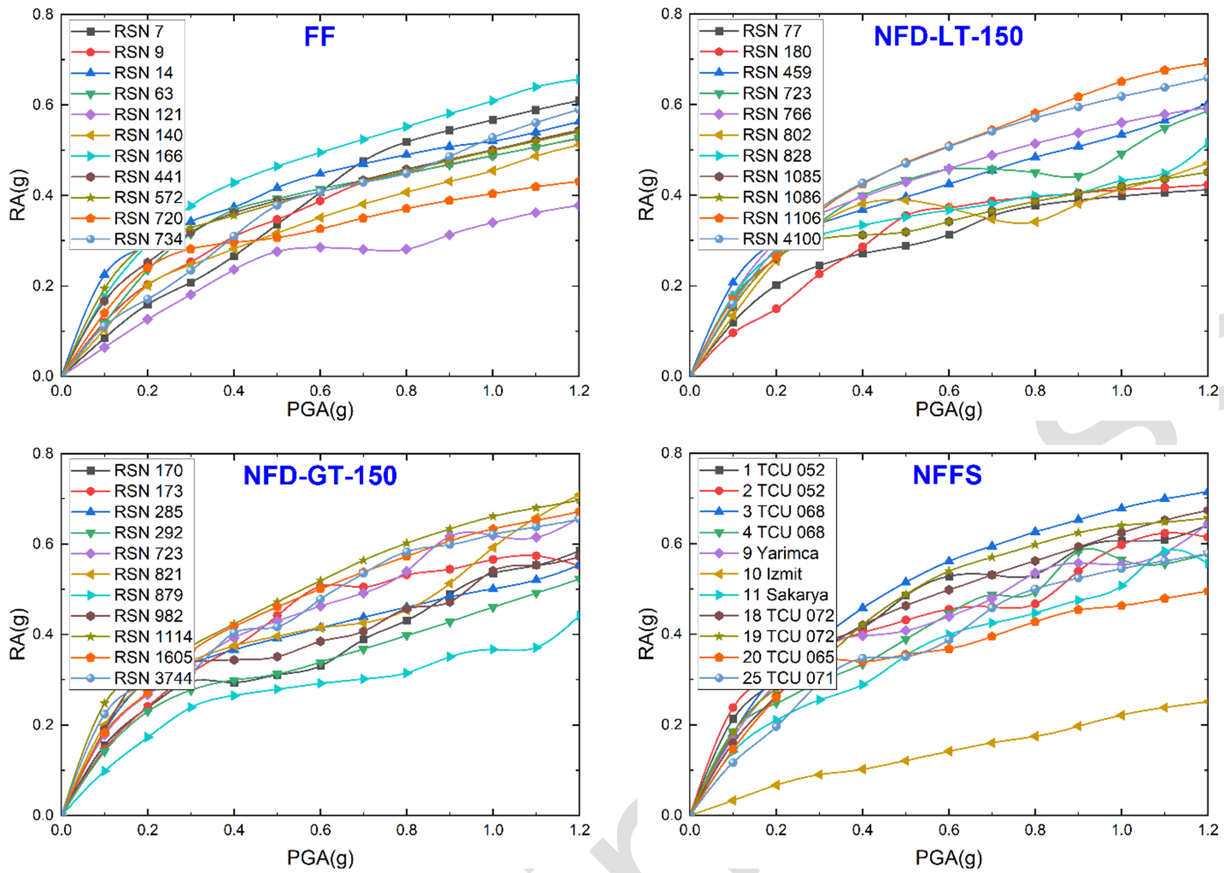

Fig. 9. IDA curves of roof accelerations (RA) for the BI building

NFD-LT-150, POE for FB reaches 95.16 % for moderate, 22.64 % for extensive, and 0.08 % for collapse at 0.8g PGA, while in the BI case the values are 0.26 %, 0 %, and 0 %, indicating near-complete mitigation. Under NFD-GT-150, POE for FB increases to 98.94 % for moderate, 79.76 % for extensive, and 26.12 % for collapse, whereas for BI the values are 75.7 %, 30.95 %, and 4.54 %, showing reduced but notable vulnerability. Under NFFS, POE for FB is 80.57 % for moderate, 56.72 % for extensive, and 30.01 % for collapse, while for BI they are 55.72 %, 28.22 %, and 9.74 %, suggesting fling-step effects increase roof drift risk.

The fragility curves for RDR_{max} demonstrate a marked escalation in vulnerability for FB under NFD-GT-150 and NFFS, with POE surpassing 75 % for moderate damage at a 0.8g PGA, consistent with IDA-recorded peaks of 6 % and 8 % RDR_{max}, respectively, indicating significant roof instability. In contrast, the BI case exhibits a reduced POE, such as 4.54 % for collapse under NFD-GT-150, which correlates with IDA's observed RDR_{max} of 0.6 %, though the elevated POE under NFFS suggests a constraint in isolation efficacy under fling-step loading. The progressive POE increment across damage states in BI highlights a persistent damping benefit; however, the influence of near-field pulses necessitates design modifications, including enhanced FPB stiffness, to ensure roof stability beyond a PGA threshold of 0.6g.

4.2.3. Roof acceleration (RA_{max})

The RA_{max} fragility curves in Fig. 14 reveal acceleration vulnerability across GM types. Under FF, POE for FB and slight damage is 99.74 % at 0.2g PGA, increasing to 100 % for moderate, 97.84 % for extensive, and 99.91 % for collapse at 0.8g PGA, indicating severe acceleration

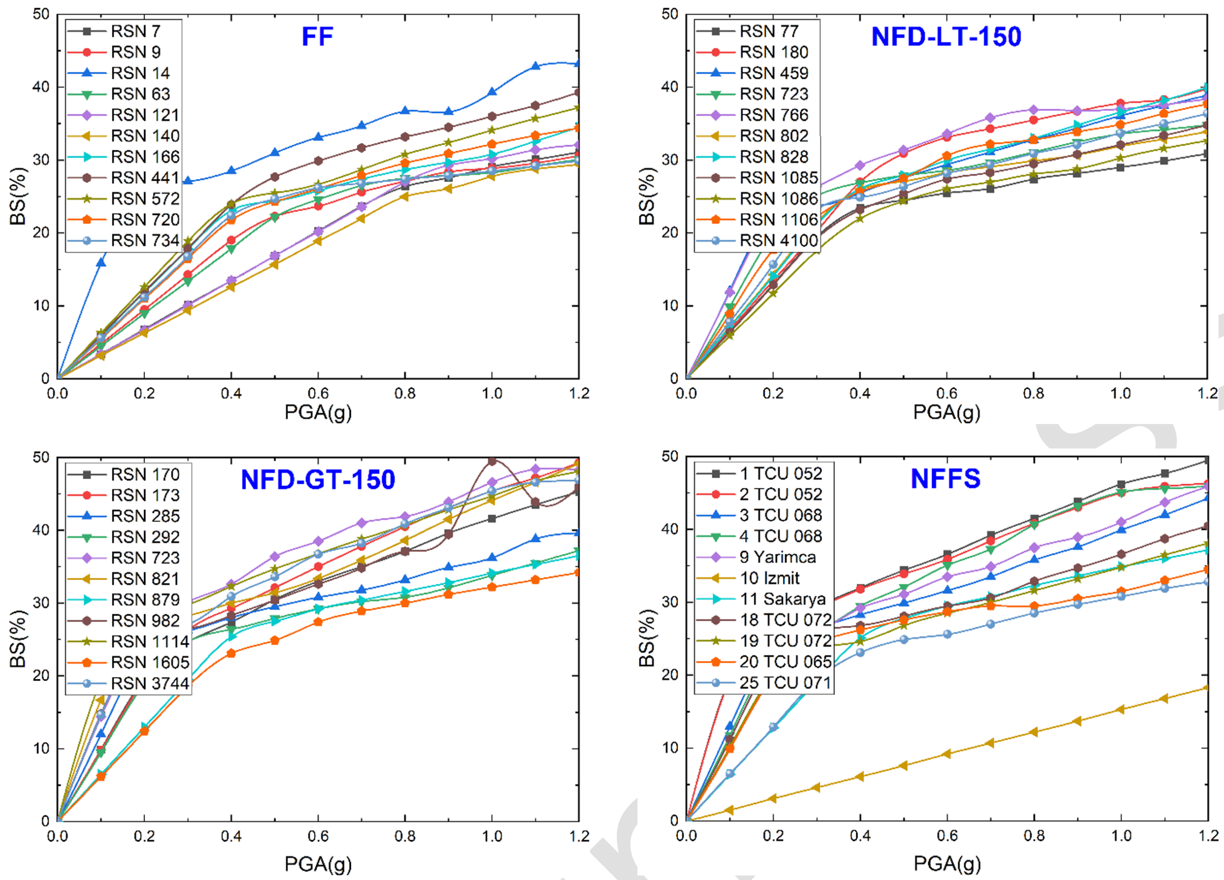

Fig. 10. IDA curves of base shear (BS) for the FB building

impact. The BI case reduces these to 98.73 %, 100 %, 97.27 %, and 69.17 %, showing partial mitigation. For NFD-LT-150, POE for FB reaches 100 % for moderate, 99.87 % for extensive, and 100 % for collapse, while for BI the values are 100 %, 99.03 %, and 77.86 %, reflecting high but controlled acceleration. Under NFD-GT-150, POE for FB is 99.96 % for moderate, 99.91 % for extensive, and 99.91 % for collapse, whereas int he BI case they are 99.05 %, 99.71 %, and 69.17 %, indicating pulse sensitivity. Under NFFS, POE for FB is 99.96 % for moderate, 99.09 % for extensive, and 95.2 % for collapse, while for BI they are 99.05 %, 89.24 %, and 67.54 %, suggesting fling-step effects elevate risk.

In the FB case, the fragility curves for RA_{max} approach 100 % POE under NFD-GT-150 and NFFS at 0.8g PGA, consistent with IDA's recorded peak of 1.4g, signifying extensive acceleration-induced structural damage. Conversely, POE for BI peaks at 69.17 % under NFD-GT-150, aligning with IDA's 0.9g peak, though it rises to 67.54 % under NFFS, indicating limitations due to pulse effects. The steep POE gradients for FB under near-field GMs underscore acceleration as a primary failure mechanism, whereas more gradual POE trends for BI reflect damping effectiveness up to 0.6g PGA, beyond which supplementary acceleration mitigation strategies may be necessary to safeguard non-structural components in regions of elevated seismic activity.

4.2.4. Maximum base shear (BS_{max})

Fig. 15 displays the BS_{max} fragility curves, illustrating the vulnerability to shear force across GM types. Under FF, POE for FB and slight damage is 99.63 % at 0.2g PGA, rising to 69.73 %

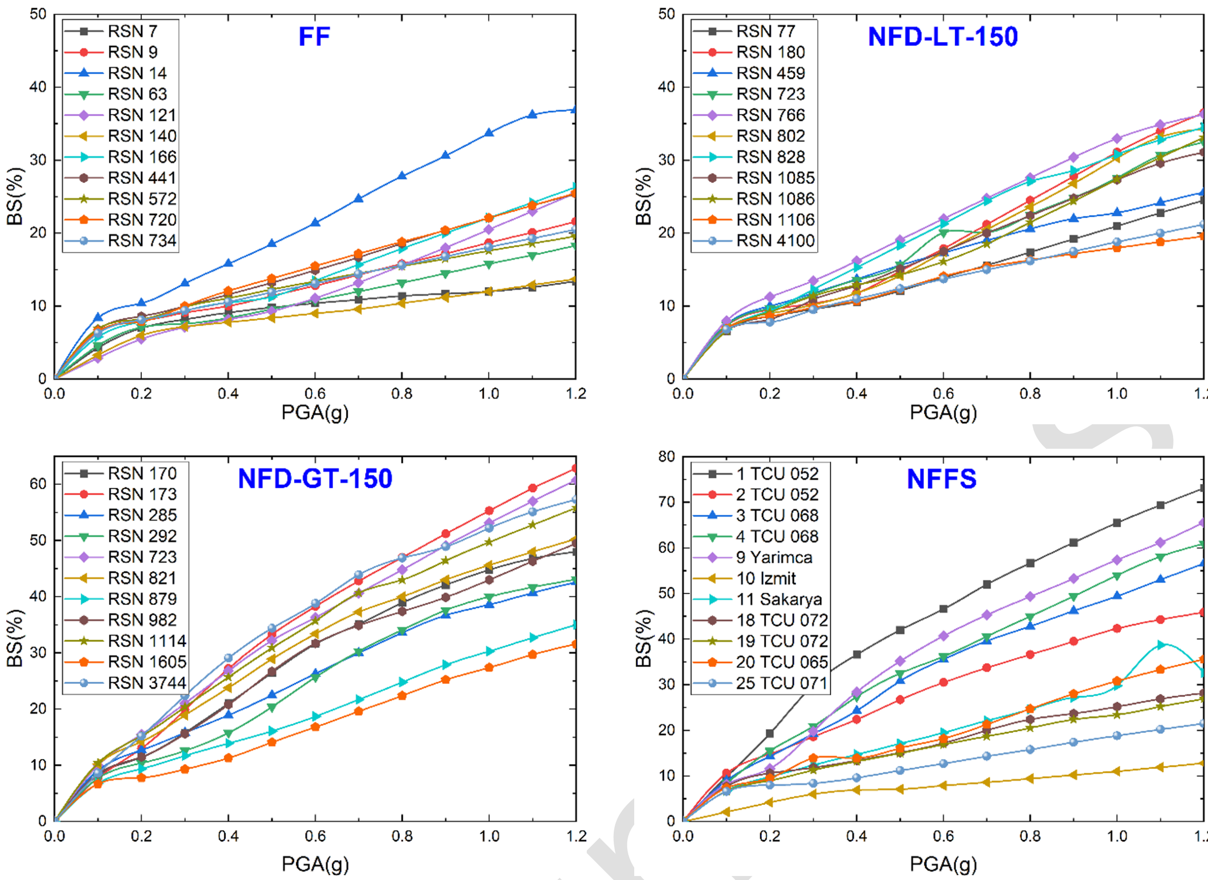

Fig. 11. IDA curves of base shear (BS) for the BI building

for moderate, 25.85 % for extensive, and 6.04 % for collapse at 0.8g PGA, indicating significant shear demand. BI reduces these to 94.30 %, 63.5 %, 10.24 %, and 0.79 %, reflecting effective mitigation. For NFD-LT-150, POE for FB reaches 100 % for moderate, 98.75 % for extensive, and 69.64 % for collapse, while for BI the values are 97.35 %, 36.06 %, and 2.37 %, showing controlled shear. Under NFD-GT-150, POE for FB is 100 % for moderate, 99.9 % for extensive, and 68.9 % for collapse, whereas in the BI case they are 99.92 %, 92.98 %, and 18.97 %, indicating pulse influence. Under NFFS, POE for FB is 99.7 % for moderate, 96.33 % for extensive, and 86.76 % for collapse, while for BI they are 98.11 %, 89.58 %, and 75.07 %, suggesting that the fling-step effects increase shear risk.

In the FB case, the fragility curves for BS_{max} exceed 68 % POE for collapse under NFD-GT-150 and NFFS at 0.8g PGA, aligning with IDA's recorded peaks of 60 % and 80 %, respectively, signifying a substantial potential for shear-induced failure. In contrast, POE for BI peaks at 18.97 % under NFD-GT-150, correlating with IDA's 50 % peak, though it increases to 75.07 % under NFFS, highlighting sensitivity to pulse effects. The curves indicate that FB's shear demand surges markedly beyond 0.6g PGA, whereas BI exhibits a more gradual increase, reflecting sustained damping efficacy; however, near-field pulses compromise this capacity. This observation underscores the need for enhanced FPB design, potentially incorporating increased friction coefficients or supplementary damping devices, to effectively mitigate shear forces in seismically active, fault-proximate regions.

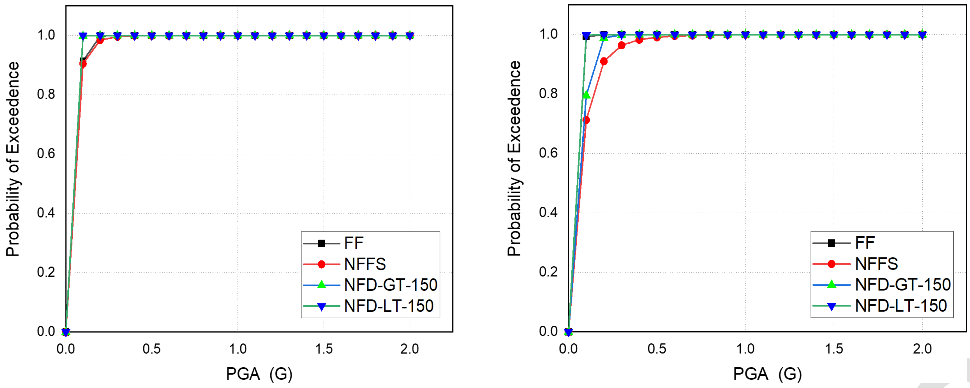

(a) slight

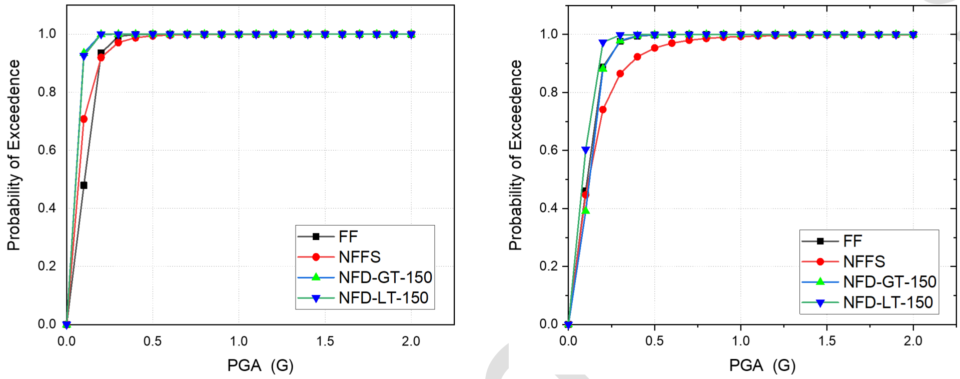

(b) moderate

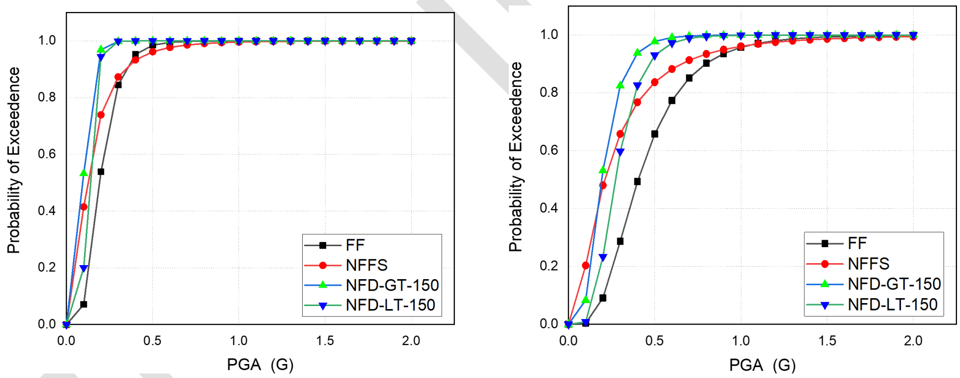

(c) extensive

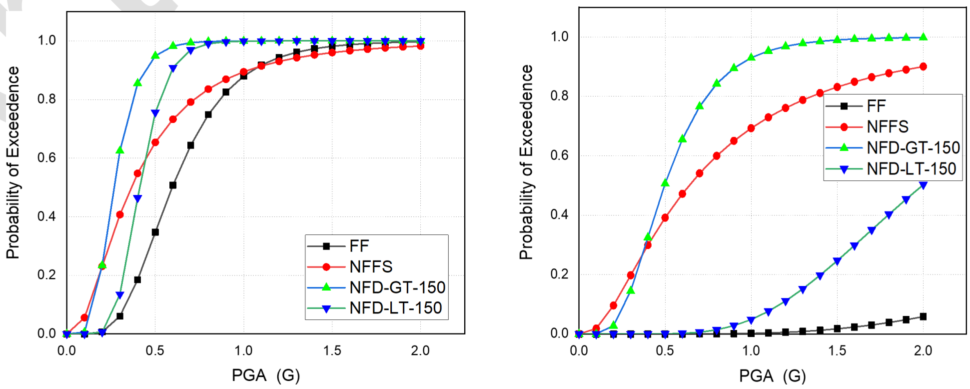

(d) collapse

Fig. 12. Comparison of fragility curves for IDR_{max} for the FB (*left*) and BI (*right*) building

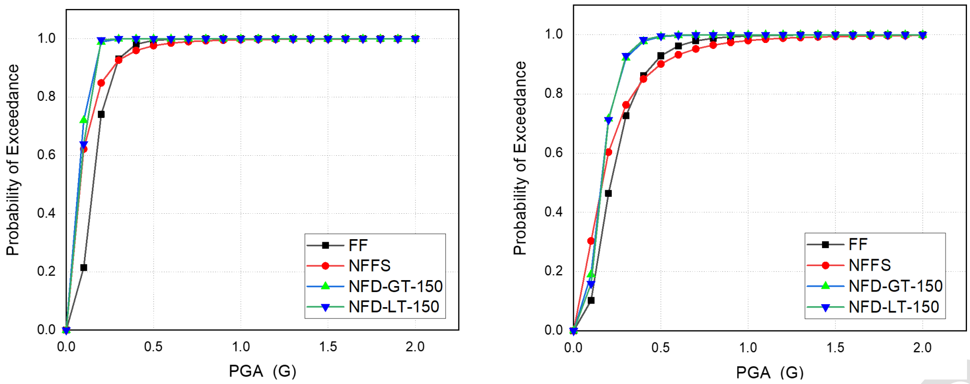

(a) slight

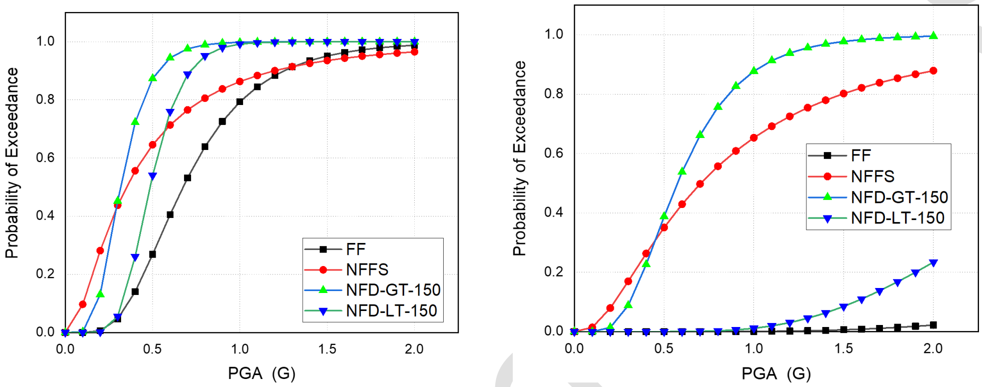

(b) moderate

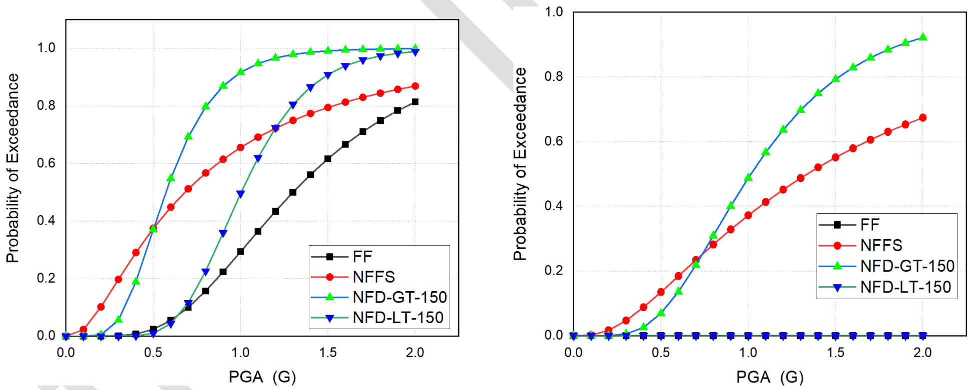

(c) extensive

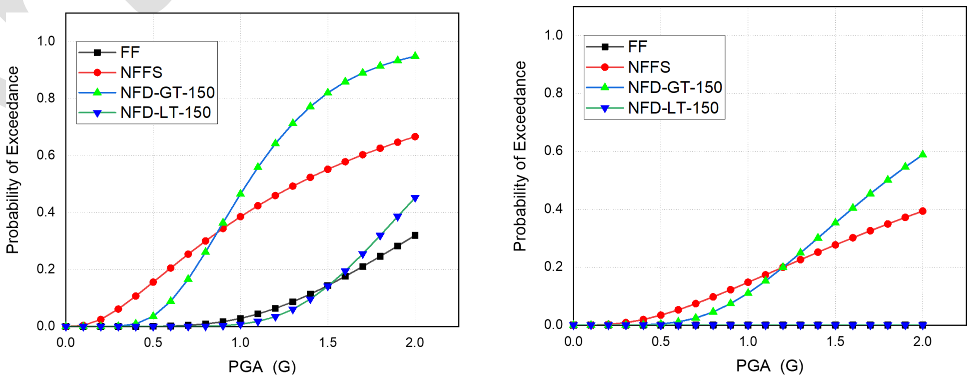

(d) collapse

Fig. 13. Comparison of fragility curves for RDR_{max} for the FB (*left*) and BI (*right*) buildings

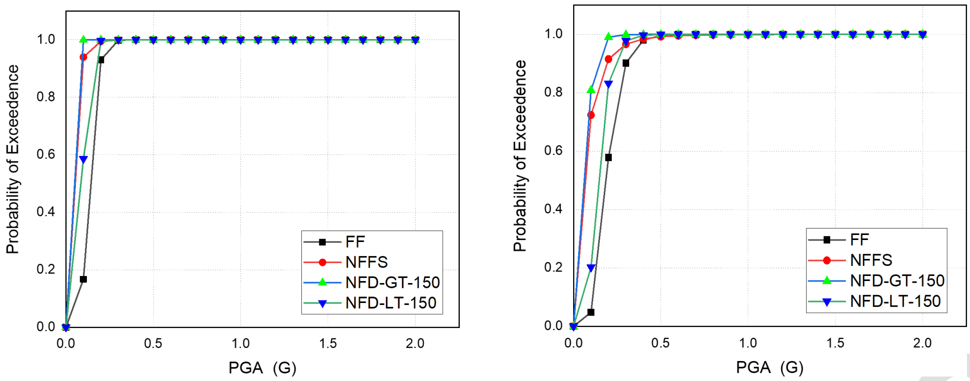

(a) slight

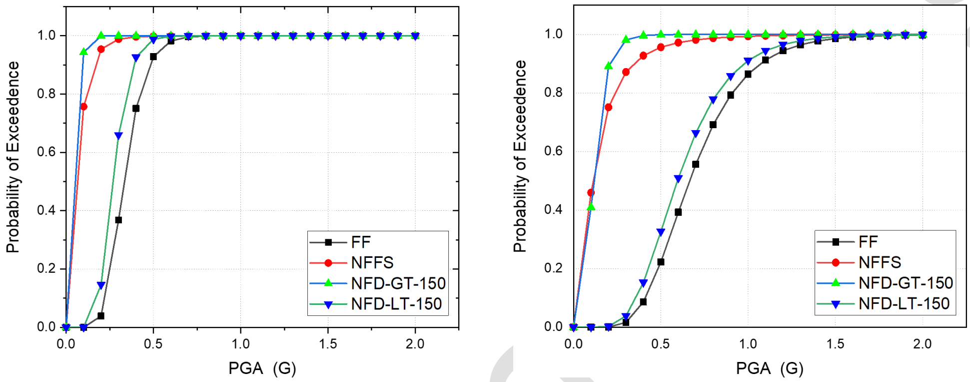

(b) moderate

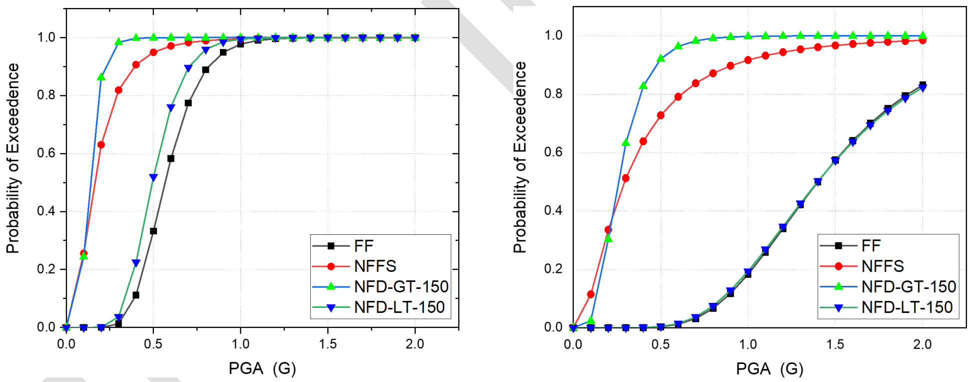

(c) extensive

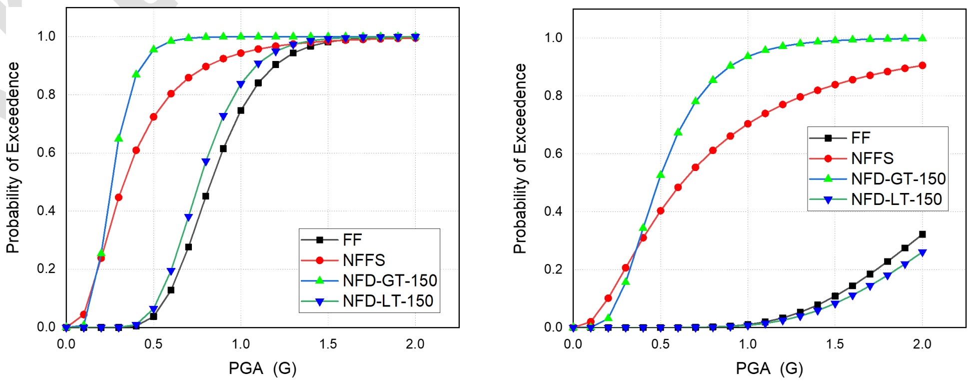

(d) collapse

Fig. 14. Comparison of fragility curves for RA_{max} for the FB (*left*) and BI (*right*) buildings

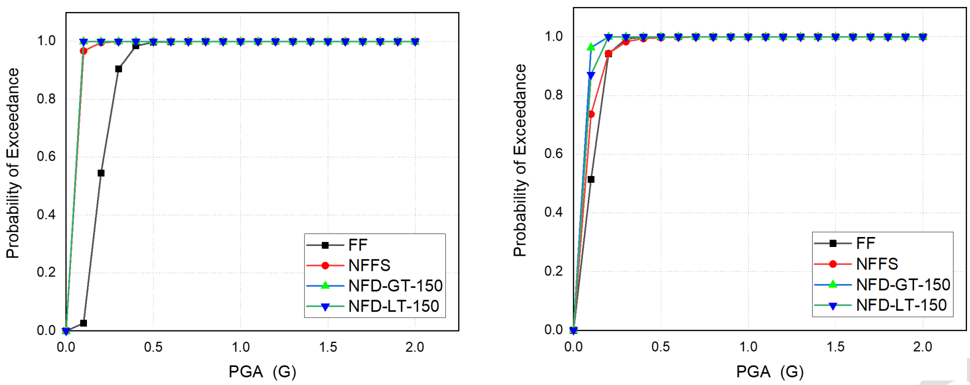

(a) slight

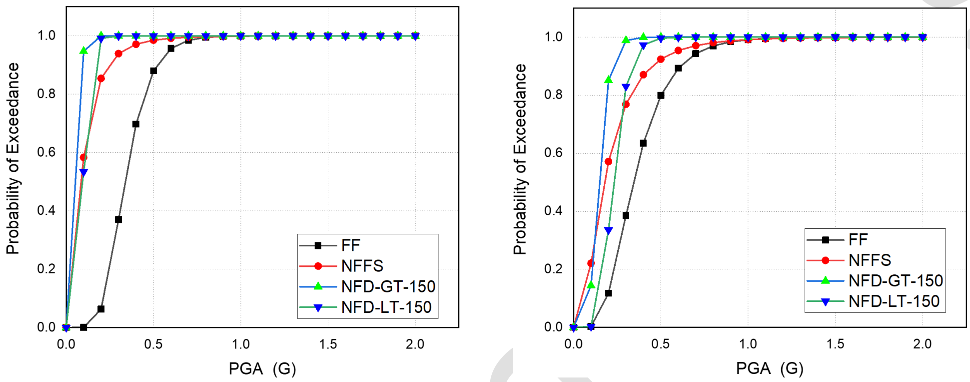

(b) moderate

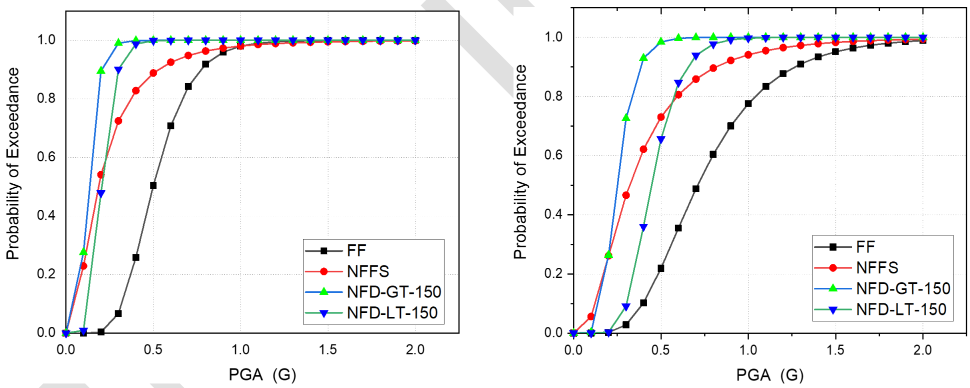

(c) extensive

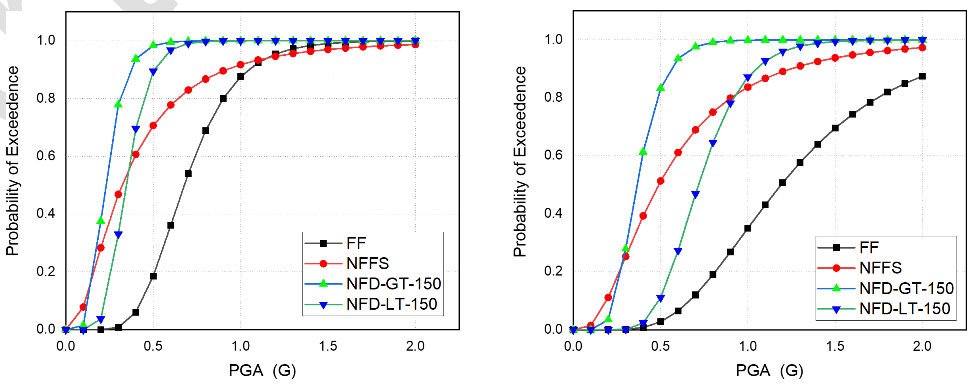

(d) collapse

Fig. 15. Comparison of fragility curves for BS_{max} for the FB (*left*) and BI (*right*) buildings

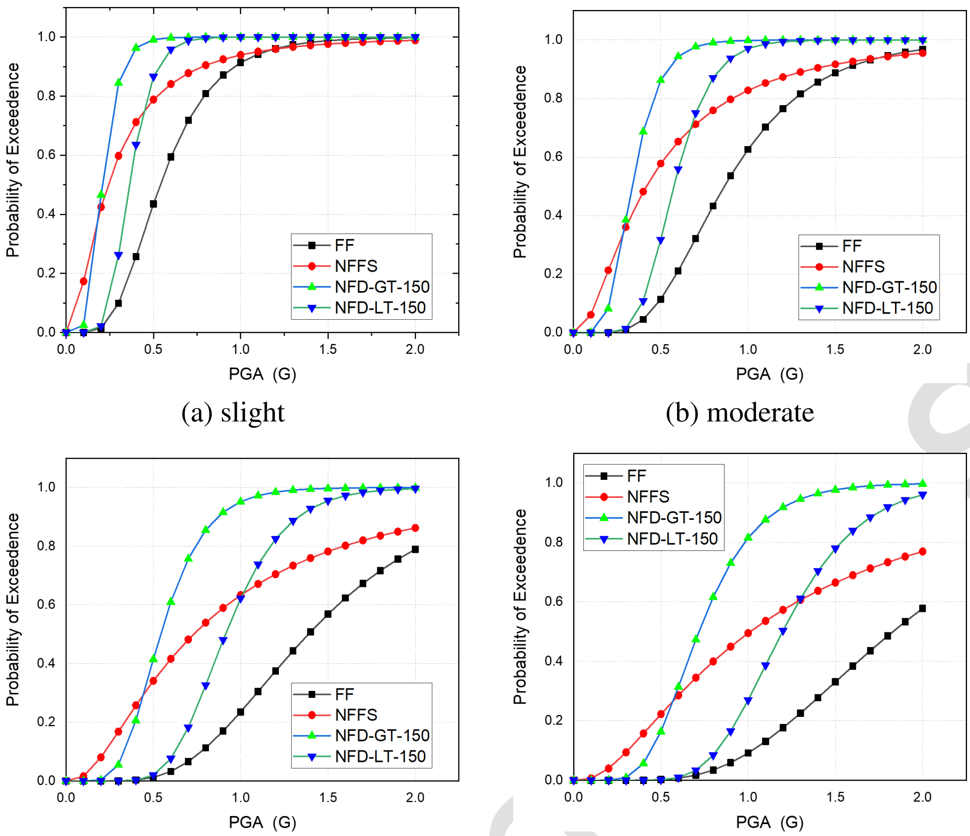

(a) slight (b) moderate

(c) extensive (d) collapse

Fig. 16. Fragility curves of ID_{max} for the BI building

4.2.5. *Maximum isolator displacement (ID_{max})*

Fig. 16 presents the ID_{max} fragility curves for BI, showing displacement vulnerability across all GM types. Under FF, POE for BI and slight damage is minimal (50 mm displacement), with moderate at 0.06 %, extensive at 0 %, and collapse at 0 %, indicating low risk. For NFD-LT-150, POE remains low, with extensive at 0 % and collapse at 0 %, reflecting controlled displacement. Under NFD-GT-150, POE for BI exceeds 150 mm for extensive (85.53 % at $0.8g$ PGA) and collapse (61.62 %), surpassing the 100 mm design displacement by 50 %, indicating significant isolator strain. Under NFFS, POE reaches 53.95 % for extensive and 39.95 % for collapse, suggesting fling-step effects push displacement limits.

The fragility curves for MID reveal that BI's displacement under NFD-GT-150 and NFFS surpasses design limits, with POE exceeding 60 % at $0.8g$ PGA, consistent with the IDA-observed strain under high-velocity pulse loading. The notably low POE under FF and NFD-LT-150, remaining below 1 %, aligns with IDA's minimal displacement recordings, validating the stability of FPBs under lower seismic intensities. The abrupt POE escalation beyond $0.6g$ PGA under near-field GMs indicates potential isolator overextension, necessitating design interventions such as optimising the curvature radius or integrating displacement stoppers to mitigate exceeding, thereby enhancing long-term reliability in seismic zones characterised by intense ground motions.

The fragility analysis confirms that near-field motions (NFD-GT-150, NFFS) pose a significantly higher risk to both structural configurations, with NFD-GT-150 producing the highest POEs across all EDPs [4]. Base isolation consistently reduced POE, with the most significant

Article in press

reductions observed for the interstorey drift ratio (up to 88.08 % in collapse state under FF at $0.2g$ PGA) and RDR_{max} (up to 99.98 % in moderate state under NFD-GT-150 at $0.8g$ PGA). However, RA_{max} and ID_{max} showed smaller reductions, particularly under NFD-GT-150, where pulse-like effects amplified accelerations and displacements [24]. These differences are statistically significant, reflecting the log-normal distribution of seismic demands [26]. Base isolation effectively mitigates structural damage, especially under FF and NFD-LT-150 motions, but its performance under NFD-GT-150 highlights the need for enhanced design considerations in near-fault regions.

5. Effect of frequency content: PGV/PGA ratio

This section investigates the impact of ground-motion frequency content, quantified by the peak ground velocity to peak ground acceleration ratio (PGV/PGA), on the seismic fragility of the FB and BI buildings. Near-field ground motions with directivity effects are categorised into high-velocity pulse-type (NFD-GT-150, PGV/PGA >150 cm/s/g) and low-velocity (NFD-LT-150, PGV/PGA <150 cm/s/g) subsets. The analysis focuses on IDR_{max} as the primary engineering demand parameter, with POE comparisons conducted at PGA levels of $0.2g$, $0.4g$, and $0.8g$, supported by fragility curve data and IDA insights.

The POE, as illustrated in Fig. 17 for FB, shows the differential impact of PGV/PGA ratios on FB seismic vulnerability. For NFD-LT-150 at $0.2g$ PGA, the POE is 97.31 % (slight), 99.99 % (moderate), 94.49 % (extensive), and 0.58 % (collapse). At $0.4g$ PGA, it increases to 99.98 % (slight), 100 % (moderate), 100 % (extensive), and 82.59 % (collapse). At $0.8g$ PGA, the POE reaches 99.99 % (slight), 99.99 % (moderate), 94.49 % (extensive), and 0.58 % (collapse). In contrast, for NFD-GT-150 at $0.2g$ PGA, the POE is 88.15 % (slight), 99.95 % (moderate), 96.91 % (extensive), and 23.40 % (collapse). At $0.4g$ PGA, it escalates to 99.59 % (slight), 100 % (moderate), 99.99 % (extensive), and 93.82 % (collapse). At $0.8g$ PGA, it shows 99.99 % (slight), 99.99 % (moderate), 97.17 % (extensive), and 99.05 % (collapse), indicating a significant escalation and near-complete vulnerability under high-velocity pulses.

For BI, Fig. 18 reveals a contrasting response. For NFD-LT-150 at $0.2g$ PGA, the POE is 97.31 % (slight), 97.31 % (moderate), 23.35 % (extensive), and 0.00 % (collapse). At $0.4g$ PGA, it increases to 99.98 % (slight), 99.98 % (moderate), 82.59 % (extensive), and 0.01 % (collapse). At $0.8g$ PGA, it reaches 99.54 % (slight), 97.31 % (moderate), 23.35 % (extensive), and 0.01 % (collapse). For NFD-GT-150 at $0.2g$ PGA, the POE is 88.15 % (slight), 98.63 % (moderate), 53.20 % (extensive), and 2.79 % (collapse). At $0.4g$ PGA, it escalates to 99.59 % (slight), 99.59 % (moderate), 93.82 % (extensive), and 32.54 % (collapse). At $0.8g$ PGA, it shows 99.81 % (slight), 98.63 % (moderate), 86.50 % (extensive), and 1.41 % (collapse), with a notable 1.40% increase in collapse POE over NFD-LT-150 at $0.8g$ PGA (1.41 % – 0.01 %), and an extensive POE difference of 63.15 % at $0.4g$ PGA (86.50% – 23.35%), highlighting pulse sensitivity.

The PGV/PGA ratio significantly influences seismic damage potential, with NFD-GT-150's high-velocity pulses increasing POE compared to NFD-LT-150 [16]. For FB, the collapse POE difference is 22.82 % at $0.2g$ PGA (23.40 % – 0.58 %), 11.23 % at $0.4g$ PGA (93.82 % – 82.59 %), and 98.47 % at $0.8g$ PGA (99.05 % – 0.58 %). For BI, the extensive POE difference is 30.85 % at $0.2g$ PGA (53.20 % – 23.35 %), 11.23 % at $0.4g$ PGA (93.82 % – 82.59 %), and 63.15 % at $0.8g$ PGA (86.50 % – 23.35 %), with collapse increasing by 2.79 % at $0.2g$ PGA (2.79 % – 0.00 %), 32.53 % at $0.4g$ PGA (32.54 % – 0.01 %), and 1.40 % at $0.8g$ PGA (1.41 % – 0.01 %). These observations highlight that the effect of the PGV/PGA ratio is significant in

Article in Press

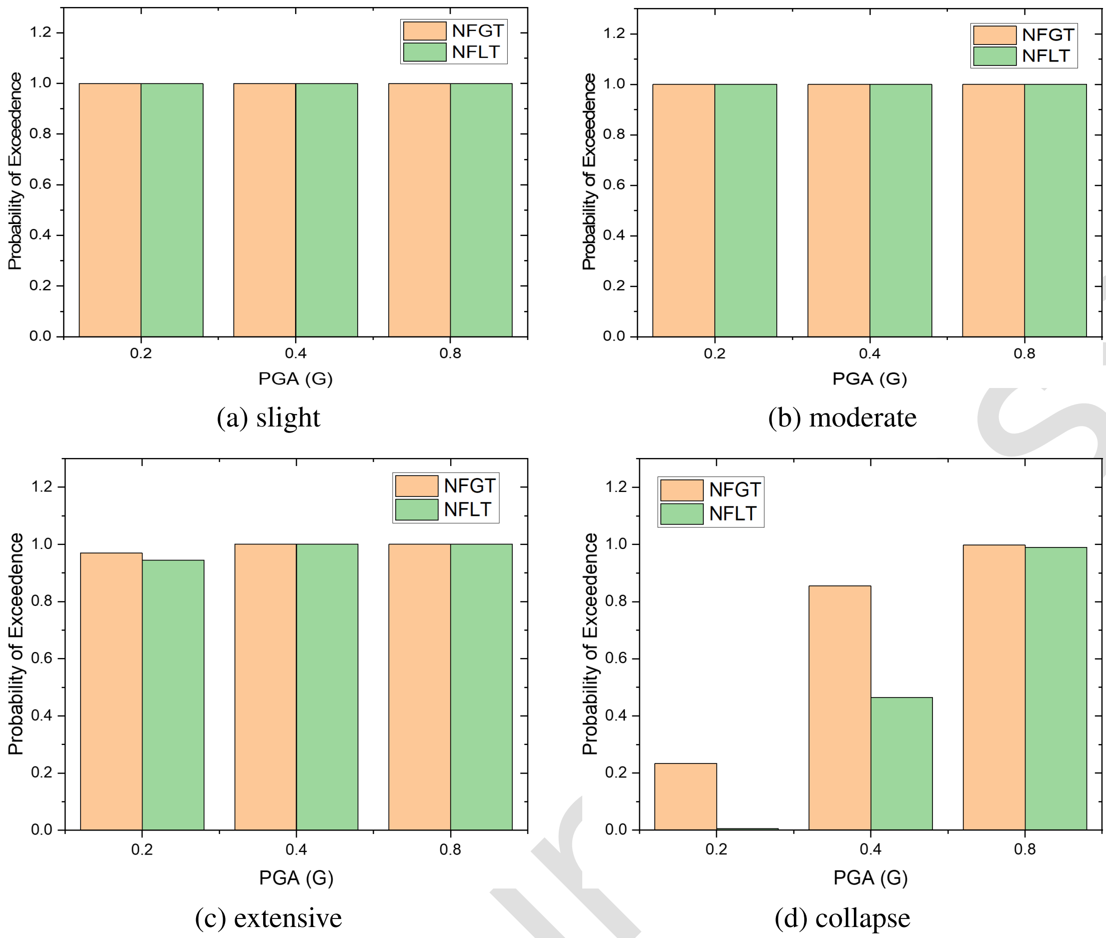

Fig. 17. POE comparison between NFD-LT-150 and NFD-GT-150 at various PGA levels for different damage states in the FB building

BI structures [4], necessitating tailored design considerations to enhance performance under pulse-dominated conditions.

6. Sensitive damage measure

This section evaluates the relative sensitivity of EDPs in assessing seismic fragility for FB and BI buildings by analysing POE for five EDPs (IDR_{max}, RDR_{max}, RA_{max}, BS_{max}, and ID_{max}) across moderate, extensive, and collapse damage states. The assessment is conducted at PGA levels of $0.2g$, $0.4g$, and $0.8g$, encompassing all GM types: FF, NFD-LT-150, NFD-GT-150, and NFFS. This analysis uses the fragility-curve results together with the corresponding IDA response trends to identify the EDP that is most sensitive to variations in seismic intensity and ground-motion type.

Table 7 presents POE values at $0.2g$ PGA, revealing IDR_{max} as the most sensitive EDP. For moderate damage under FF, IDR_{max} POE is 89 % (BI) and 94 % (FB), surpassing RA_{max} at 57.87 % (BI) and 93 % (FB), with RDR_{max} and ID_{max} showing lower values (0 % and 0.06 % for BI, respectively). Under NFD-LT-150, IDR_{max} POE reaches 97.31 % (BI) and 99.99 % (FB), compared to RA_{max} at 83.14 % (BI) and 99.67 % (FB), and ID_{max} at 0.01 % (BI). For NFD-GT-150, IDR_{max} POE is 88.15 % (BI) and 99.95 % (FB), exceeding RA_{max} at 90.44 % (BI) and 99.79 % (FB), with NFFS showing 74.11 % (BI) and 91.96 % (FB) for IDR_{max} versus 63.52 %

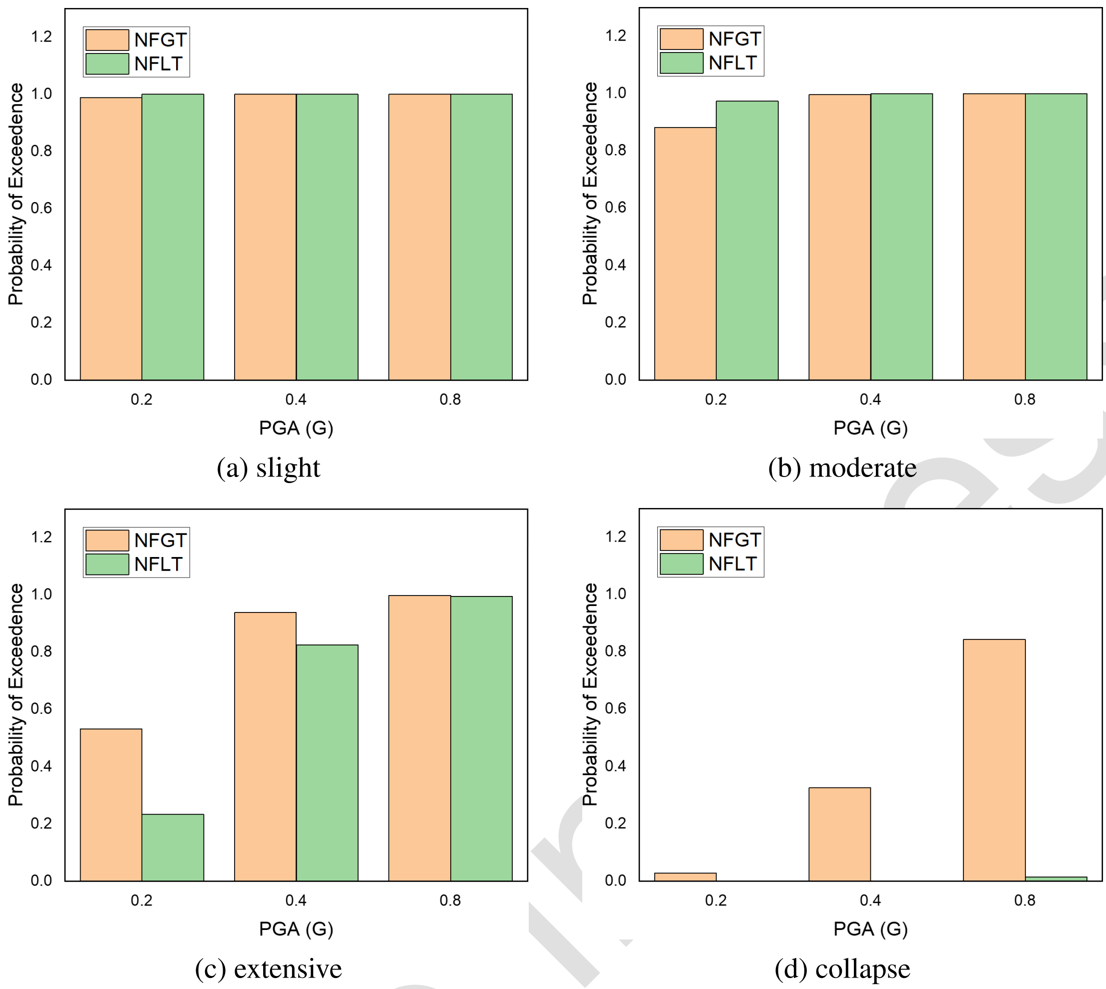

Fig. 18. POE comparison between NFD-LT-150 and NFD-GT-150 at various PGA levels for different damage states in the BI building

(BI) and 86.66 % (FB) for RA_{max}. In the extensive state under FF, IDR_{max} POE is 9.2 % (BI) and 53.9 % (FB), outperforming RA_{max} at 3.54 % (BI) and 33.74 % (FB), with NFD-GT-150 reaching 53.2 % (BI) and 96.91 % (FB) versus 15.77 % (BI) and 79.07 % (FB) for RA_{max}. For collapse under NFD-GT-150, IDR_{max} POE is 2.79 % (BI) and 23.4 % (FB), surpassing RA_{max} at 0.41 % (BI) and 25.71 % (FB), with NFFS at 9.57 % (BI) and 23.09 % (FB) versus 6.12 % (BI) and 28.43 % (FB) for RA_{max}.

At 0.4g PGA, Table 8 supports the dominance of IDR_{max}. For moderate damage under FF, IDR_{max} POE is 99.4 % (BI) and 99.9 % (FB), exceeding RA_{max} at 98.04 % (BI) and 100 % (FB), with NFD-GT-150 at 99.59 % (BI) and 100 % (FB) versus 99.93 % (BI) and 100 % (FB) for RA_{max}. Under NFFS, IDR_{max} POE is 92.31 % (BI) and 98.8 % (FB), compared to 91.08 % (BI) and 98.7 % (FB) for RA_{max}. In the extensive state, IDR_{max} POE under NFD-GT-150 is 93.82 % (BI) and 99.99 % (FB), outpacing RA_{max} at 80.94 % (BI) and 99.91 % (FB), with NFFS at 62.69 % (BI) and 85.34 % (FB) versus 59.47 % (BI) and 89.33 % (FB). For collapse, IDR_{max} POE under NFD-GT-150 is 32.54 % (BI) and 85.54 % (FB), surpassing RA_{max} at 22.23 % (BI) and 95.25 % (FB), with NFFS at 29.93 % (BI) and 54.78 % (FB) versus 29.29 % (BI) and 70.78 % (FB). The IDA correlation, with IDR_{max} peaks of 10 % (FB) versus 1.1 % (BI) under NFD-GT-150, supports this trend.

Table 9 at 0.8g PGA further validates IDR_{max} sensitivity. For moderate damage under FF,

Table 7. POEs for different damage measures and types of earthquakes at PGA of 0.2g

Earthquakes	Damage measures								
	IDR_{max}		RDR_{max}		RA_{max}		BS_{max}		ID_{max}
	BI	FB	BI	FB	BI	FB	BI	FB	BI
Moderate damage									
FF	89	94	0	0.5	57.87	93	11.7	6.3	0.06
NFFS	74.11	91.96	7.93	28.12	63.52	86.66	57.15	85.42	21.31
NFD-GT	88.15	99.95	1.39	13.08	90.44	99.79	85.14	99.97	8.2
NFD-LT	97.31	99.99	0	0.16	83.14	99.67	33.57	99.13	0.01
Extensive damage									
FF	9.2	53.9	0	0	3.54	33.74	0.3	0.4	0
NFFS	32.43	57.75	1.65	10.16	22.35	55.07	26.14	54.09	8.06
NFD-GT	53.2	96.91	0.03	0.47	15.77	79.07	26.45	89.53	0.35
NFD-LT	23.35	94.49	0	0	10.55	69.62	0.33	47.84	0
Collapse damage									
FF	0	0.7	0	0	0.06	3.89	0	0	0
NFFS	9.57	23.09	0.23	2.18	6.12	28.43	11.11	28.34	3.97
NFD-GT	2.79	23.4	0	0	0.41	25.71	3.47	37.65	0.02
NFD-LT	0	0.58	0	0	0.24	14.63	0	3.75	0

Table 8. POEs for different damage measures and types of earthquakes at PGA of 0.4g

Earthquakes	Damage measures								
	IDR_{max}		RDR_{max}		RA_{max}		BS_{max}		ID_{max}
	BI	FB	BI	FB	BI	FB	BI	FB	BI
Moderate damage									
FF	99.4	99.9	0	14.02	98.04	100	63.5	69.73	4.48
NFFS	92.31	98.8	26.33	55.63	91.08	98.7	87.05	97.12	48.18
NFD-GT	99.59	100	22.62	72.29	99.93	100	99.92	100	68.7
NFD-LT	99.98	100	0	26.08	99.7	100	97.35	100	10.82
Extensive damage									
FF	49.3	95.2	0	0.73	52.33	97.84	10.24	25.85	0.31
NFFS	62.69	85.34	8.79	29.06	59.47	89.33	62.15	82.81	25.76
NFD-GT	93.82	99.99	2.59	18.91	80.94	99.91	92.98	99.9	20.64
NFD-LT	82.59	100	0	0.11	70.63	99.87	36.06	98.75	0.24
Collapse damage									
FF	0	18.47	0	0	8.63	75.07	0.79	6.04	0.04
NFFS	29.93	54.78	1.9	10.66	29.29	70.78	39.29	60.69	15.75
NFD-GT	32.54	85.54	0.08	0.93	22.23	95.25	61.34	93.75	5.67
NFD-LT	0.01	46.42	0	0	15.24	92.66	2.37	69.64	0

Article in Press

Table 9. POEs for different damage measures and types of earthquakes at PGA of 0.8g

Earthquakes	Damage measures								
	IDR_{max}		RDR_{max}		RA_{max}		BS_{max}		ID_{max}
	BI	FB	BI	FB	BI	FB	BI	FB	BI
Moderate damage									
FF	99.99	100	0.01	63.9	99.99	100	96.98	99.47	43.25
NFFS	98.63	99.9	55.72	80.57	99.05	99.96	98.11	99.7	75.94
NFD-GT	100	100	75.7	98.94	100	100	100	100	99.1
NFD-LT	100	100	0.26	95.16	100	100	100	100	87.1
Extensive damage									
FF	90.27	99.94	0	15.74	97.27	100	60.47	91.87	11.26
NFFS	86.5	97.17	28.22	56.72	89.24	99.09	89.58	96.33	53.95
NFD-GT	99.86	100	30.95	79.76	99.71	100	99.98	100	85.53
NFD-LT	99.54	100	0	22.64	99.03	100	97.73	100	32.61
Collapse damage									
FF	0.05	74.85	0	0.89	69.17	99.91	18.97	68.9	3.42
NFFS	59.99	83.54	9.74	30.01	67.54	95.2	75.07	86.76	39.95
NFD-GT	84.3	99.78	4.54	26.12	86.76	100	99.16	99.96	61.62
NFD-LT	1.41	99.05	0	0.08	77.86	100	64.66	99.75	8.43

IDR_{max} POE is 99.99 % (BI) and 100 % (FB), matching RA_{max} at 99.99 % (BI) and 100 % (FB), with NFD-GT-150 at 100 % for both, though RDR_{max} lags at 75.7 % (BI). In the extensive state, IDR_{max} POE under NFD-GT-150 is 99.86 % (BI) and 100 % (FB), exceeding RA_{max} at 99.71 % (BI) and 100 % (FB), with NFFS at 86.5 % (BI) and 97.17 % (FB) versus 89.24 % (BI) and 99.09 % (FB). For collapse, IDR_{max} POE under NFD-GT-150 is 84.3 % (BI) and 99.78 % (FB), surpassing RA_{max} at 86.76 % (BI) and 100 % (FB), with NFFS at 59.99 % (BI) and 83.54 % (FB) versus 67.54 % (BI) and 95.2 % (FB). IDA's RA_{max} peaks of 1.4g (FB) versus 0.9g (BI) under NFD-GT-150 complement this, though the ID_{max} value of 61.62 % (BI) under NFD-GT-150 highlights isolator-specific risk.

The statistical analysis of POE trends across PGA levels identifies IDR_{max} as the most sensitive EDP, with the highest POE values (e.g., 99.95 % for FB under NFD-GT-150 at 0.2g PGA, 99.99 % at 0.4g, 100 % at 0.8g) reflecting its direct linkage to structural deformation and failure modes. RA_{max} ranks second, with POE variability (e.g., 99.79 % for FB vs. 90.44 % for BI under NFD-GT-150 at 0.2g PGA) indicating acceleration sensitivity, particularly under near-field GMs. ID_{max}, with POE up to 61.62 % (BI) under NFD-GT-150 at 0.8g PGA, is critical for isolator performance but less indicative of global collapse. RDR_{max}, with POE peaking at 75.7 % (BI) under NFD-GT-150 at 0.8 g PGA, exhibits lower sensitivity. This hierarchy, supported by IDA's deformation trends (e.g., IDR_{max} of 10 % for FB vs. 1.1 % for BI), advocates for IDR_{max} as the primary EDP in seismic design codes, such as ASCE 41 [1], with RA_{max} as a secondary metric for non-structural safety.

Article in Press

7. Conclusion

This study conducted a case-study-based probabilistic seismic performance assessment of a representative 10-storey RC frame in fixed-base and friction-pendulum base-isolated configurations under far-field, near-field directivity, and near-field fling-step earthquake motions. IDA and PSDM were used to develop fragility curves for five EDPs: maximum interstorey drift ratio (IDR_{max}), maximum roof drift ratio (RDR_{max}), maximum isolator displacement (ID_{max}), maximum roof acceleration (RA_{max}), and maximum base shear (BS_{max}) across four damage states: slight, moderate, extensive, and collapse. The key findings are:

1. Vulnerability to near-field earthquakes: Both fixed-base and base-isolated frames exhibited significantly higher probabilities of exceedance (POE) under near-field motions (NFD and NFFS) due to velocity pulses and directivity effects, which increased seismic demand across all damage states.
2. Impact of the PGV/PGA ratio: The PGV/PGA ratio emerged as a critical indicator of damage potential. Near-field earthquakes with PGV/PGA >150 cm/s/g (NFD-GT-150) produced higher POE than those with PGV/PGA <150 cm/s/g (NFD-LT-150), with differences most pronounced in extensive and collapse states (e.g., 32.54 % higher collapse POE for base-isolated under NFD-GT-150 vs. NFD-LT-150 at $0.4g$ PGA).
3. Effectiveness of base isolation: Base isolation reduced IDR_{max} by up to 88.08 % in the collapse state under FF at $0.2g$ PGA, demonstrating significant mitigation for far-field motions. However, its effectiveness diminished under NFD-GT-150 due to its high energy content, while remaining beneficial under NFD-LT-150, substantially reducing structural damage.
4. Variability of POE across damage states: POE variability across ground-motion types was minimal in the slight damage state but increased significantly in moderate to collapse states, reflecting the growing influence of ground-motion characteristics on structural vulnerability as damage severity escalated.
5. Sensitive damage measures: IDR_{max} and ID_{max} were the most sensitive EDPs, consistently showing the highest POE in moderate, extensive, and collapse states across all earthquake types. These metrics should be prioritised in the seismic design and evaluation of base-isolated structures, particularly under near-field motions with high PGV/PGA ratios (>150 cm/s/g).

These findings, statistically validated through the log-normal distribution of seismic demands [25], emphasise the need to incorporate PGV/PGA metrics and near-field effects into seismic design codes like IS 1893 (2016) [13] to enhance the resilience of base-isolated structures in near-fault regions. Future research should explore soil-structure interaction and irregular building configurations to further refine design practices.

The present study is limited to one representative 10-storey regular RC frame analysed in fixed-base and friction-pendulum base-isolated configurations. Therefore, the results should be interpreted as a detailed case-study-based fragility assessment rather than as generalized conclusions for all RC buildings. The seismic response of shorter or taller frames may differ because of changes in fundamental period, stiffness distribution, modal participation, higher-mode effects and interaction between the structural period, isolation period, and dominant pulse period of near-fault ground motions. Shorter frames may show higher acceleration and base-shear sensitivity because of their relatively higher stiffness, whereas taller frames may exhibit stronger higher-mode effects and different drift distributions. Therefore, future studies should

Article in Press

extend the present IDA-PSDM-based fragility framework to a wider range of low-rise, mid-rise, and high-rise RC frames, including different plan configurations, isolation properties, and three-dimensional structural models.

References

[1] ASCE/SEI 41-17 – Seismic evaluation and retrofit of existing buildings, American Society of Civil Engineers, 2017.

[2] Bakhshi, A., Mostafavi, S. A., Development of fragility curves for base-isolated RC structures, Proceeding of the 9th International Conference on Structural Dynamic, Porto, 2014, pp. 2 947–2 953.

[3] Bhagat, S., Wijeyewickrema, A. C., Seismic response evaluation of base-isolated reinforced concrete buildings under bidirectional excitation, Earthquake Engineering and Engineering Vibration 16 (2017) 365–382. https://doi.org/10.1007/s11803-017-0387-8

[4] Bhandari, M., Bharti, S. D., Shrimali, M. K., Datta, T. K., Seismic fragility analysis of base-isolated building frames excited by near-and far-field earthquakes, Journal of Performance of Constructed Facilities 33 (3) (2019) 4019029. https://doi.org/10.1061/(ASCE)CF.1943-5509.0001298

[5] Cornell, C. A., Krawinkler, H., Progress and challenges in seismic performance assessment, PEER Center News 3 (2000) 1–3.

[6] Dhanani, N., Thoriya, A., Rangwala, H., Vora, T., Dhankot, M., A Bayesian Monte Carlo framework for risk-targeted seismic separation gaps in adjacent fixed-base and base-isolated buildings, Journal of Building Pathology and Rehabilitation 11 (2026) No. 91. https://doi.org/10.1007/s41024-025-00768-5

[7] Ebrahimi, S., Naderpour, H., Zahrai, S. M., Comprehensive evaluation of seismic fragility in base-isolated buildings enhanced with supplemental dampers considering pounding phenomenon, Structures 68 (2024) No. 107077. https://doi.org/10.1016/j.istruc.2024.107077

[8] FEMA 356 FE – Prestandard and commentary for the seismic rehabilitation of buildings, Federal Emergency Management Agency, Washington, D.C., 2000.

[9] Fenz, D. M., Constantinou, M. C., Behaviour of the double concave friction pendulum bearing, Earthquake Engineering & Structural Dynamics 35 (11) (2006) 1 403–1 424. https://doi.org/10.1002/eqe.589

[10] Habib, A., Al Houri, A., Yildirim, U., Comparative study of base-isolated irregular RC structures subjected to pulse-like ground motions with low and high PGA/PGV ratios, Structures 31 (2021) 1 053–1 071. https://doi.org/10.1016/j.istruc.2021.02.021

[11] He, P., Ma, Y., Liu, C., Seismic resilience assessment of base-isolated structures with friction pendulum isolation bearings based on two-dimensional fragility, Journal of Building Engineering 103 (2025) No. 112202. https://doi.org/10.1016/j.jobe.2025.112202

[12] IS 456 – Plain and reinforced concrete, Indian Standard, Bureau of Indian Standards, Dehli, 2000.

[13] IS 1893 – Part-1. Criteria for earthquake resistant design of structures, Part 1: General provisions and buildings, Indian Standard, Bureau of Indian Standards, New Delhi, 2016.

[14] Jangid, R. S., Computational numerical models for seismic response of structures isolated by sliding systems, Structural Control and Health Monitoring 12 (1) (2005) 117–137. https://doi.org/10.1002/stc.59

[15] Jangid, R. S., Optimum friction pendulum system for near-fault motions, Engineering Structures 27 (3) (2005) 349–359. https://doi.org/10.1016/j.engstruct.2004.09.013

Article in Press

[16] Jangid, R. S., Kelly, J. M., Base isolation for near-fault motions, Earthquake Engineering & Structural Dynamics 30 (5) (2001) 691–707. https://doi.org/10.1002/eqe.31

[17] Kang, Y., Zhang, Z., Zhang, Z., Zhang, X., Liu, Q., Optimal design and seismic performance of base-isolated structures with varying heights equipped with tuned inerter dampers subjected to far-fault and near-fault ground motions, Applied Sciences 15 (9) (2025) No. 4739. https://doi.org/10.3390/app15094739

[18] Liu, C., Fang, D., Yan, Z., Seismic fragility analysis of base-isolated structure subjected to near-fault ground motions, Periodica Polytechnica Civil Engineering 65 (3) (2021) 768–783. https://doi.org/10.3311/PPci.15276

[19] Majdi, A., Kontoni, D.-P. N., Almujibah, H., Correlation of the near-fault pulse-like ground motion characteristics with the vulnerability of buildings, Buildings 14 (9) (2024) No. 2801. https://doi.org/10.3390/buildings14092801

[20] Mazza, F., Mazza, M., Nonlinear seismic analysis of irregular r.c. framed buildings base-isolated with friction pendulum system under near-fault excitations, Soil Dynamics and Earthquake Engineering 90 (2016) 299–312. https://doi.org/10.1016/j.soildyn.2016.08.028

[21] Naeim, F., Kelly, J. M., Design of seismic isolated structures: From theory to practice, John Wiley & Sons, 1999. https://doi.org/10.1002/9780470172742

[22] Nazarnezhad, T., Naderpour, H., Probabilistic damage evaluation of base-isolated reinforced concrete structures under near-fault pulse-like bidirectional seismic excitations, Structures 32 (2021) 1 156–1 170. https://doi.org/10.1016/j.istruc.2021.02.025

[23] Pacific Earthquake Engineering Research Center, https://ngawest2.berkeley.edu/.

[24] Petti, L., Polichetti, F., Lodato, A., Palazzo, B., Modelling and analysis of base-isolated structures with friction pendulum system considering near fault events, Open Journal of Civil Engineering 3 (2) (2013) 86–93. http://dx.doi.org/10.4236/ojce.2013.32009

[25] Porter, K., Kennedy, R., Bachman, R., Creating fragility functions for performance-based earthquake engineering, Earthquake Spectra 23 (2) (2007) 471–489. https://doi.org/10.1193/1.2720892

[26] Shivachandra, A., Shiv, V., Bharti, D., Kumar, M., Tushar, S., Datta, K., Seismic behaviour of FPS – Isolated frames under the action of mainshock and aftershocks, Journal of Vibration Engineering & Technologies 12 (2024) 3 399–3 415. https://doi.org/10.1007/s42417-023-01053-w

[27] Sitapra, N. J., Shukla, K. P., Asodariya, C. M., Thoriya, A. J., Incremental dynamic analysis of geometrically irregular RCC buildings, In: Sustainable building materials and construction, Lecture Notes in Civil Engineering Vol. 222, Springer, Singapore, 2022, pp. 247–253. https://doi.org/10.1007/978-981-16-8496-8_32

[28] Sitapra, N. J., Shukla, K. P., Vora, T. P., Thoriya, A. J., Use of IDA to estimate variations in drift demands of irregular RCC buildings, In: Recent advances in materials, mechanics and structures, Lecture Notes in Civil Engineering Vol. 269, Springer, Singapore, pp. 85–95. https://doi.org/10.1007/978-981-19-3371-4_8

[29] Somerville, P. G., Development of an improved representation of near fault ground motions, SMIP98 – Seminar on Utilization of Strong-Motion Data, vol. 15, Oakland, California, 1998.

[30] Sun, Q., Dias, D., Significance of Rayleigh damping in nonlinear numerical seismic analysis of tunnels, Soil Dynamics and Earthquake Engineering 115 (2018) 489–494. https://doi.org/10.1016/j.soildyn.2018.09.013

[31] Thomas, T., Mathai, A., Study of base isolation using friction pendulum bearing system, IOSR Journal of Mechanical and Civil Engineering 2006 (2016) 19–23.

[32] Thoriya, A., Rangwala, H., Vora, T., Dhankot, M., Comparative seismic assessment of base-isolated and fixed-base RC buildings: Integrating fragility, sensitivity, and dependence under near-

Article in Press

and far-fault motions, Asian Journal of Civil Engineering 27 (2025) 1 559–1 581. https://doi.org/10.1007/s42107-025-01576-5

[33] Vamvatsikos, D., Cornell, C. A., Applied incremental dynamic analysis, Earthquake Spectra 20 (2) (2004) 523–553. https://doi.org/10.1193/1.1737737

[34] Vamvatsikos, D., Cornell, C. A., Incremental dynamic analysis, Earthquake Engineering & Structural Dynamics 31 (3) (2002) 491–514. https://doi.org/10.1002/eqe.141

[35] Vibhute, A. S., Bharati, S. D., Shrimali, M. K., Datta, T. K., Optimum coefficient of friction in FPS for base isolation of building frames, Practice Periodical on Structural Design and Construction 27 (4) (2022) No. 4022042. https://doi.org/10.1061/(ASCE)SC.1943-5576.0000722

[36] Wang, B., Karavasilis, T. L., Chen, P., Dai, K., Seismic modeling and performance evaluation of seismically isolated building considering large strain effects under near-fault earthquakes, Journal of Building Engineering 90 (2024) No. 109339. https://doi.org/10.1016/j.jobe.2024.109339

[37] Zayas, V. A., Low, S. S., Mahin, S. A., A simple pendulum technique for achieving seismic isolation, Earthquake Spectra 6 (2) (1990) 317–333. https://doi.org/10.1193/1.1585573

Article in Press